6300-EN-01

DEPARTMENT OF CIVIL ENGINEERING
UNIVERSITY OF AALBORG
SOHNGAARDSHOLMSVEJ 57 DK-9000 AALBORG DENMARK
TELEPHONE +45 - 98142333 TELEX 69523 auciv dk TELEFAX +45 - 98142555

U.S. Army Research
Development & Standardization Group, UK
Att.: Fiscal Office
223 Marylebone Road
London NW1 5TH
England

Sept. 6, 1990
HFB/bt

Dear Sirs

Re.: Research contract R & D 6300-EN-01 "Development of design methods for breakwater armour units" ref. no. DAJA 45-89-M-0406

Final report

The research has been completed in accordance with the research proposal dated 1. May 1989.

The research program contained the following activities:

1) Coordination of the armour unit research at the Hydraulics Laboratory of the University of Aalborg (AHL) and CERC.
2) Investigation of static load in tests on sloping ramps. Comparison of results from 200 kg concrete units (AHL) with results from 200 g units made of concrete (AHL) and epoxy material (CERC) with the objective of studying size scale effects and surface roughness scale effects.
3) Investigation of the possibility of measuring impact loads in model tests with the small scale units (200 g).
4) Wave tank parametric studies of the dependence of the armour unit stresses on sea state parameters and the geometry of the breakwater. The wave tank tests are coordinated with tests at CERC, cf. item 1. AND
5) Establishment of design diagrams including proposal for improvement of Dolosse.

(ER)

90

Item 1., 2. and 3 were reported in 1st Interim Report of November 29, 1989.

The present final report summarizes the results from all five items. The full comprehensive report entitled "On the determination of concrete armour unit stresses including specific results related to Dolosse" is enclosed. This report contains also a historical review of armour unit stress research as well as a general discussion of research methods. Moreover, some of the important results from the CERC, Crescent City Prototype Study, are included where it is relevant. These parts of the report is the contribution of Mr. G.L. Howell, CERC.

Summary of main results

1. A complete coordinated detailed program for wavetank parametric studies of dolosse with 4 different waist ratios has been completed. The tests at CERC will include a 1 : 50 slope foreshore while the tests at AHL will include a 1 : 20 slope foreshore. Otherwise the set up and the test procedure will be identical. A detailed program is produced.

2. The ramp tests with large scale units (200 kg) and the small scale units (200 g) have been completed at AHL.

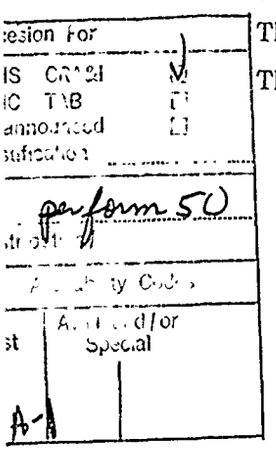

The main results are given in Figs. 1., 2. and 3.

The conclusions are the following:

- The results with the 200 g units on ramps (compaction experiment) compare well with the results obtained with 200 g units when differences in surface roughness and applied compaction are taken into account. Thus the small scale tests provide reliable results with respect to static stresses.
- The negligence of shear and axial force components in the small scale units introduces only minor errors which can be accounted for.
- The surface roughness influences the static stresses. Correction can be introduced.

3. Dynamic pendulum and drop tests were performed with the 200 g instrumented dolosse and the results compared with the results of similar prototype tests (1.5t - 20t dolosse) earlier performed by H.F. Burcharth. Example of the main results are given in Fig. 4.

   As seen from the Figures the following can be concluded:

- The stress response of the small scale units to dynamic loads follows the impact scaling law valid for homogeneous prototype concrete units, i.e. $\sigma \sim \sqrt{\lambda}$, where λ is the length scale. Necessary sampling rate is app. 6,000 Hz per signal.
- It is possible to determine the calibration factor which makes it possible to convert the small scale impact recordings to prototype stresses.
- Thus it should be possible in small scale flume tests to record also the impact generated stresses provided the sampling rate is high enough. The last point can be solved as it is only a question of computer capacity.

4. Tests with instrumented 200 g Dolosse were performed in a wave flume. The test set-up is shown in Fig. 5. Examples of main results are given in Figs. 6, 7, 8 and 9.

   As seen from the Figures the following can be concluded:

   - The distribution of peaks of static plus pulsating stresses (i.e. total stresses ex. impact stresses) follows closely the ln-normal distribution. Fig. 6.
   - The static stresses are almost independent of the wave height and of the position of the Dolosse within each armour unit layer. Dolosse in the top layer exhibit smaller static stresses than those in the bottom layer. Static stresses dominates over pulsating stresses when looking at average figures, Fig. 7.
   - The distribution of the pulsating stresses in stationary sea states follows the Rayleigh distribution quite closely, Fig. 8. This indicates that a frequency domain response analysis might be possible as an alternative method of producing design diagrams.
   - The pulsating stress (in terms of an upper fractile value) increases linearly with the significant wave height. The stresses in the bottom layer are approximately the double of those in the bottom layer, Fig. 9.

5. The results mentioned under items 2-4 provides the basis for the design diagram as presented in Fig. 10.
   The diagram is the first design diagram for a complex type of armour unit which is based on a comprehensive test program and as such applicable for professional use. The reason for denoting it a preliminary design chart is, that impact stress contributions, which are relevant only in case of application of non-conservative hydraulic design criteria, has not been implemented because impact stress results from flume tests have not been studied yet and

are not included in the present program. However, under the present program it has been demonstrated that it is possible to implement impact stresses, cf. item 3. Moreover, the stress contribution from flukes are not included in Fig. 10 because it depends very much on the applied definition of the failure of a Dolosses. Some designers do not accept that one or two flukes breaks while others might accept this because the Dolosse still has a high residual capacity. However, corrections can be made to Fig. 10 by the use of the approximative upper and lower limits found from ramp tests as represented in Fig. 11.

Finally it should be mentioned that the results of the ongoing coordinated tests at CERC should be merged with the present results, thus giving a wider parametric basis for a design diagram.

Sincerely yours

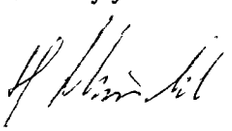

Hans F. Burcharth
Prof. of Marine Civil Engineering

Slope : 1 in 0.9, 1.38, 2. Instrumented Dolos position: 1 and 2.
- - - : Fracture limitation of concrete Dolosse (density 2300 kg/m^3, tensile strength 3 5 MPa)
- - - : 200 g concrete Dolos (without shear and axial forces)
- - - : 200 kg concrete Dolos (without shear and axial forces)

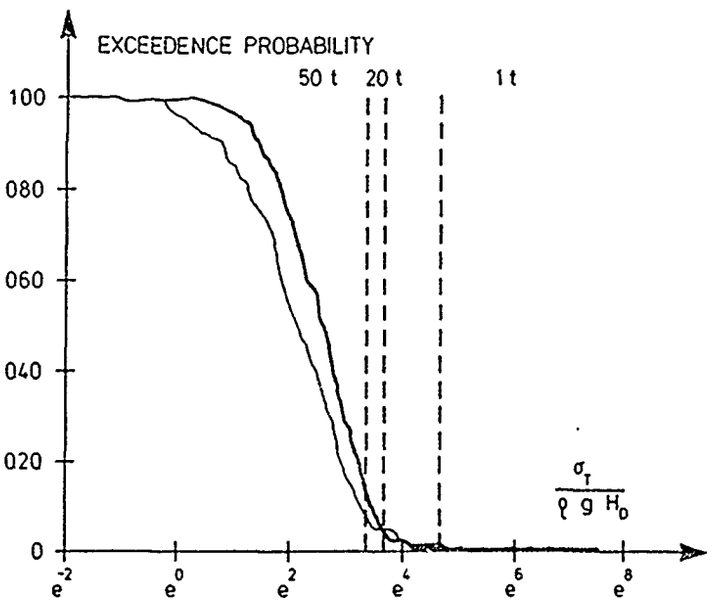

Fig. 1. Comparison of stress distributions in shank cross sections of 200 kg and 200 g concrete Dolosse armour. Influence from shear and axial forces are neglected. AHL experiments.

Slope : 1 in 0.9, 1.38, 2. Instrumented Dolos position 1, 2
- - - : Fracture limitation of concrete Dolosse
(density 2300 kg/m³, tensile strength 3.5 MPa)
— · — : Exceedence probability

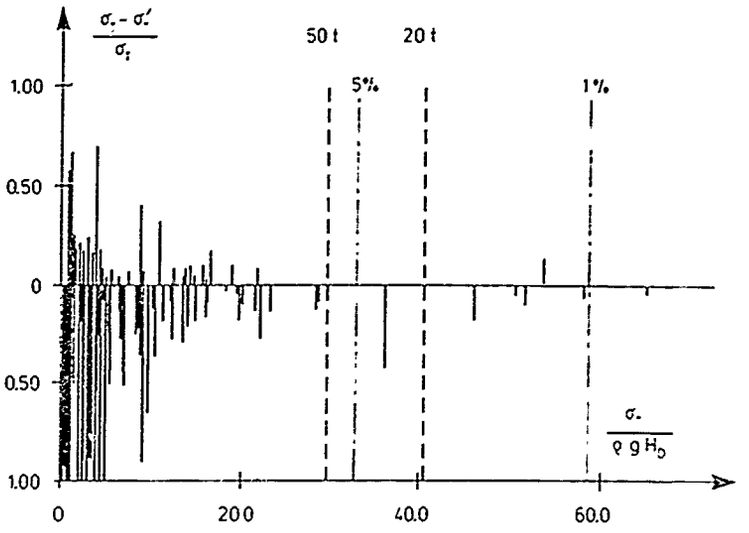

Fig. 2. Example of stress contribution from axial and shear forces. Tests with 200 kg Dolosse, AHL experiments.

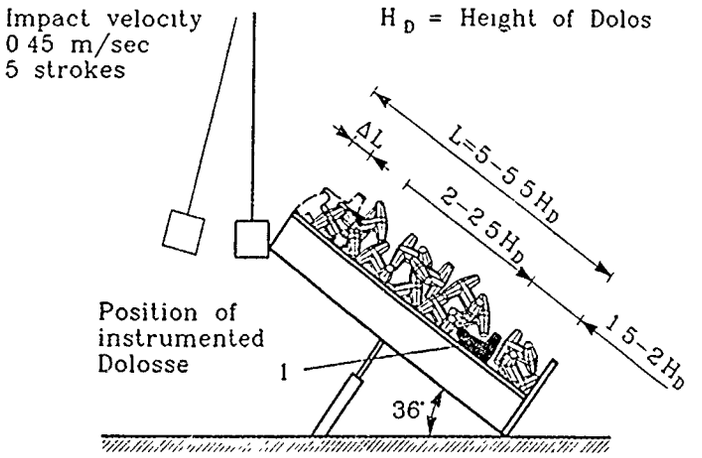

compacting weight in kg	Average of σ_T (MPa) in shank cross section of smooth units (polyester)	rough units (concrete)
1	0.031	0.022
2	0.033	0.026
3	0.039	0.028

Fig. 3. Influence of layer settlement on Dolos stress (results are not corrected for the small difference in armour unit densities).

σ_T : Max principle tensile stress
E : Modulus of elasticity
ρ . Concrete density
H_D : Dolos height
h : Lifted height of gravitational centre of Dolos (in drop test) or pendulum (in pendulum test)
r : Dolos waist ratio

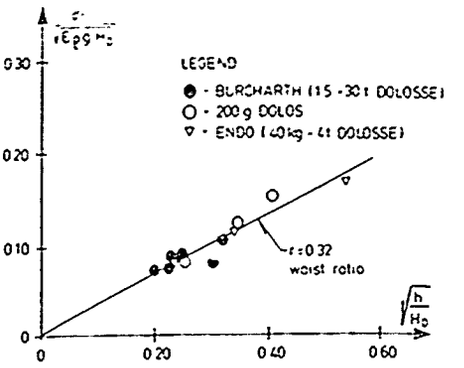

a) Drop tests

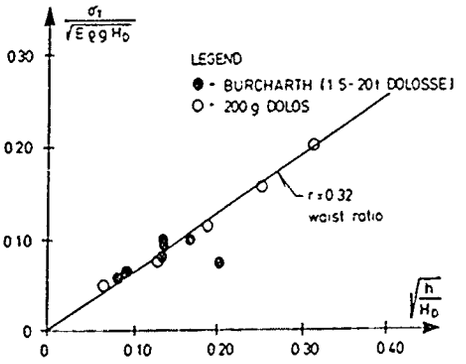

b) Pendulum tests

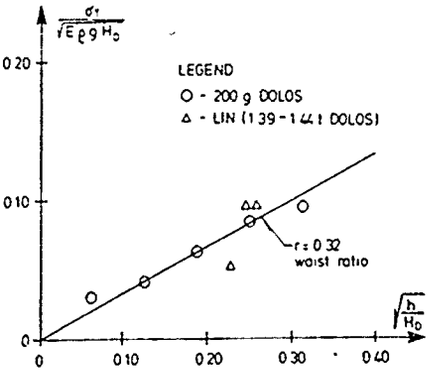

c) Transverse pendulum tests

Fig. 4. The result of impact calibration.

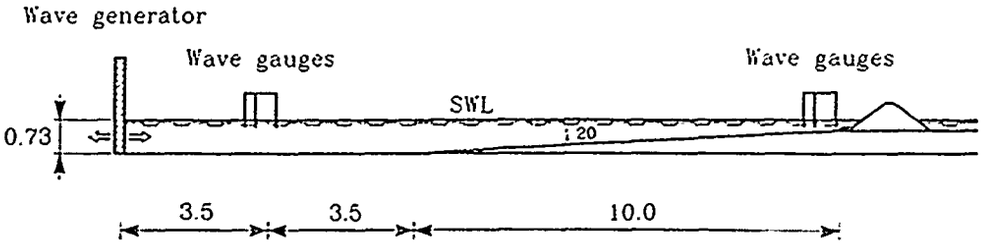

Set-up of the wave flume

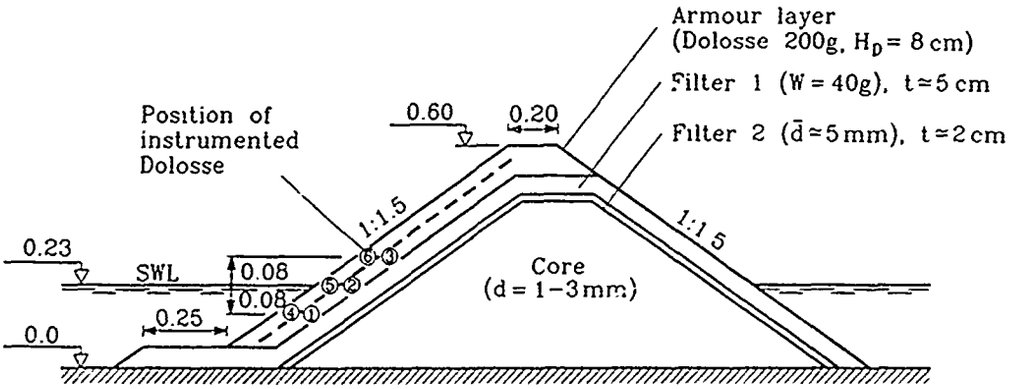

Cross section of the breakwater

Measures and levels in meter

Fig. 5. Set-up of the wave flume and the cross section of the breakwater. AHL experiments.

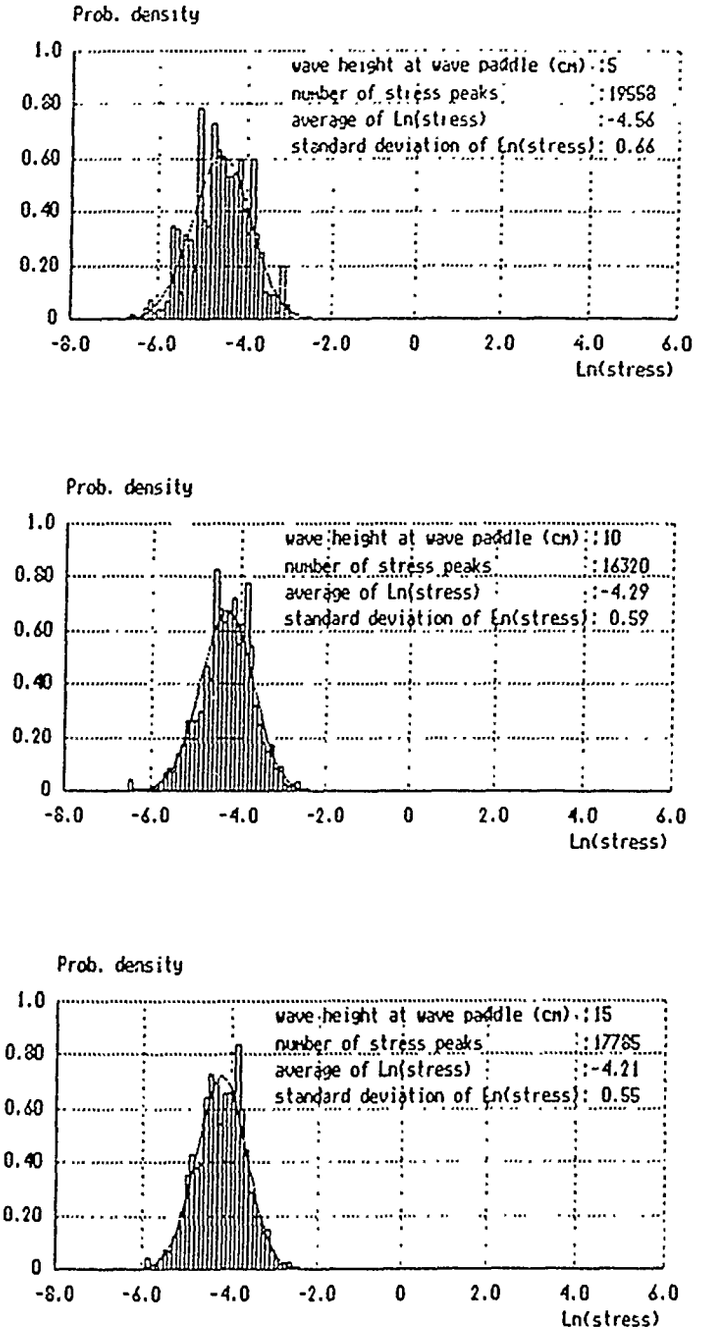

Fig. 6. Distribution of peaks static and pulsating stresses (in MPa).

	Pos. No of Dolosse / H^p_{m0} cm / $\bar{\sigma}_{static}/\bar{\sigma}$	5		10		15	
bottom layer	1	$\frac{0.015}{0.016}$	1.0	$\frac{0.016}{0.019}$	0.89	$\frac{0.017}{0.021}$	0.81
	2	$\frac{0.017}{0.019}$	0.89	$\frac{0.016}{0.021}$	0.76	$\frac{0.016}{0.023}$	0.70
	3	$\frac{0.014}{0.015}$	0.93	$\frac{0.017}{0.022}$	0.77	$\frac{0.018}{0.027}$	0.67
top layer	4	$\frac{0.009}{0.011}$	0.82	$\frac{0.009}{0.012}$	0.75	$\frac{0.01}{0.013}$	0.77
	5	$\frac{0.012}{0.016}$	0.75	$\frac{0.013}{0.018}$	0.72	$\frac{0.012}{0.018}$	0.67
	6	$\frac{0.006}{0.007}$	0.86	$\frac{0.007}{0.009}$	0.78	$\frac{0.008}{0.011}$	0.73

$\bar{\sigma}_{static}$ Average static stresses in 20 tests. The static stress is defined as the average of the static recorded before and after the wave action.
$\bar{\sigma}$ Average of peaks of total stresses in 20 tests.
The Dolosse positions are shown in Fig. 24.

Fig. 7. Relative importance of static stresses in flume tests with 200 g Dolosse as recorded in one shank cross section.

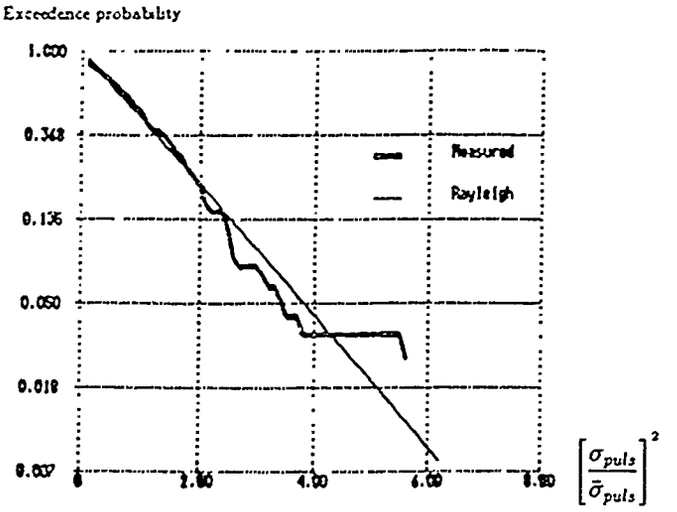

Fig. 8. Example of distribution of pulsating stress wave heights in a stationary sea state (short term distribution). Flume tests with 200 g Dolosse at AHL.

Dolosse pos. / H^t_{m0} (cm) / $\bar{\sigma}_{puls\,1/10}$ (MPa)	bottom layer			top layer		
	1	2	3	4	5	6
5.7	0.006	0.0051	0.0061	0.0035	0.0038	0.0018
11.8	0.013	0.014	0.022	0.0071	0.008	0.0097
17.9	0.018	0.018	0.028	0.011	0.011	0.014

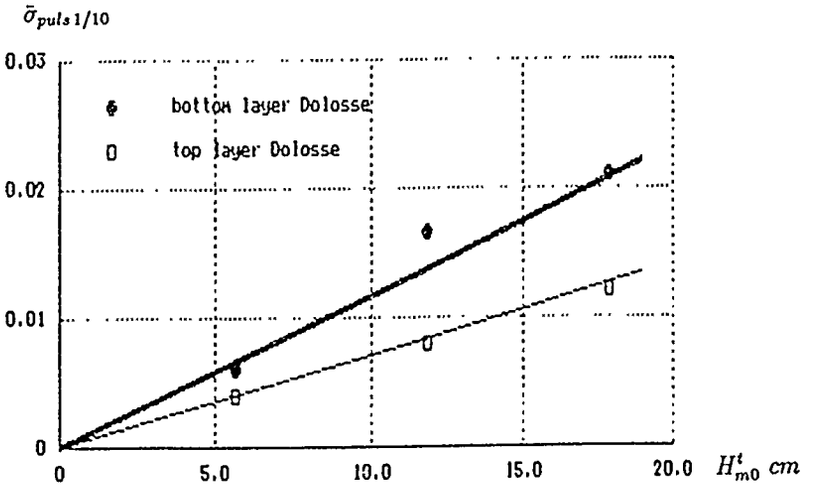

Fig. 9. Pulsating stress dependency on wave climate and Dolosse position. Flume tests with 200 g Dolosse at AHL.

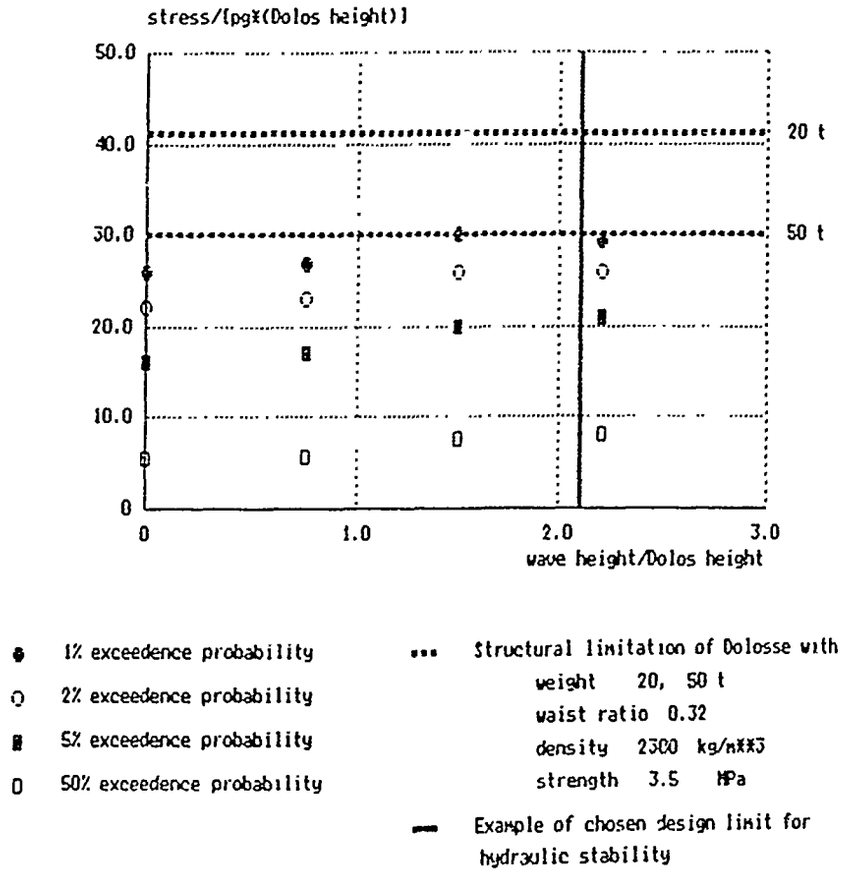

Fig. 10. Preliminary design chart for Dolos with waist ratio 0.32. The design chart covers the area between levels SWL ± app. 1.5 times the Dolos height. The exceedence probabilities are obtained from the fitted log-normal distribution of peaks of static and pulsating stresses. Impact stress, fatigue and the stress contribution from flukes are not included.

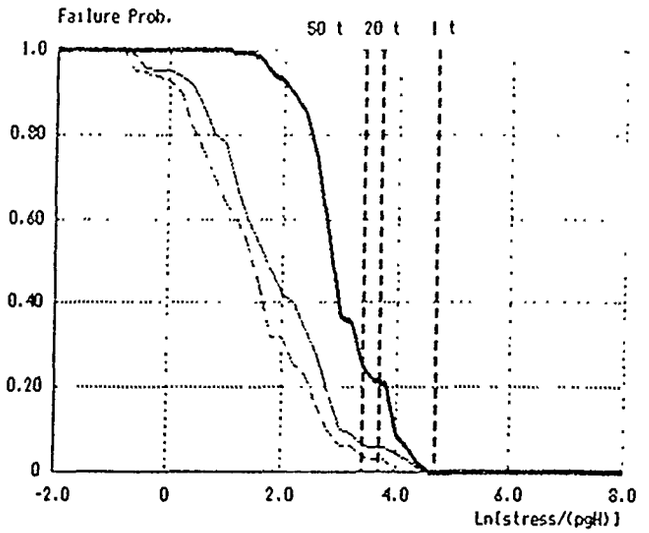

— Simple upper bound of Dolos failure probability
(assuming no correlation of failures in flukes and shanks)

— Failure probability of shank
(Simple lower bound of Dolos failure probability)

--- Failure probability of fluke

••• Structural limitation of Dolosse with
weight 1, 20 and 50 t
waist ratio 0.32
density 2300 kg/mXX3
strength 3.5 MPa

Results from 200 kg Dolos ramp tests, axial and shear forces included

Instrumented Dolos positions 1 and 2

Slope of ramp 1:0.9, 1:1.33 and 1:2

Sample size 124 stresses in shank and fluke sections respectively

Fig. 11. Failure probability of Dolosse based on recorded static stresses in ramp tests in the dry, AHL experiments.

Research contract R & D 6300-EN-01
"Development of design methods for breakwater armour units"
ref. no. DAJA 45-89-M-0406.

Report.

CONTENTS

On the determination of concrete armour unit stresses including specific results related to Dolosse

H.F. Burcharth[1] Gary L. Howell[2] Liu Zhou[3]

Abstract

Failures of rubble mound breakwaters armoured with complex types of unreinforced armour units are often due to breakage of the units. This happens when the stresses exceeds the material strength. Sufficient parametric studies of the stresses are not yet available to produce design diagrams for structural integrity.

The paper presents a general discussion of the problems related to stress determination and describes the results and the analyses of model tests with 200 kg and 200 g load cell instrumented Dolosse. Static stresses, wave generated stresses and stresses due to impacts were studied as well as model and scale effects. Moreover, some results from the Crescent City prototype Dolosse study are presented and related to results from small scale model tests.

A preliminary design diagram for Dolosse is presented as well.

Introduction

Many of the recent dramatic failures of a number of large rubble mound breakwaters armoured with Dolosse and Tetrapods were caused by breakage of the concrete armour units. Breakage took place before the hydraulic stability of intact units in the armour layers expired. Thus there was not a balance between the strength (structural integrity) of the units and the hydraulic stability (resistance to displacements) of the armour layer. Although the relative strength of the units decreases with increasing size (Burcharth 1980) the shape of the units was kept constant and not related to the size of the units and the size was not increased beyond the demand dictated by the hydraulic stability.

[1]Prof. of Marine Civil Engineering, Aalborg University, Denmark

[2]Acting Senior Research Engineer. U.S. Army Corps of Engineers, Coastal Engineering Research Center, Waterways Experiment Station, Vicksburg, Miss., USA

[3]Ph.D., visiting researcher, Aalborg University, Denmark

While the hydraulic stability can be roughly estimated by formulae and further evaluated in conventional hydraulic model tests, it is much more complicated to assess the structural integrity of the armour units. The increased research activity in this field has not yet resulted in generally applicable design diagrams or formulae by which the armour units can be designed as is the case for other civil engineering structural members.

The goal is a procedure for the estimation of the armour unit stresses in a specific structure as function of the sea state, in other words, we are seeking the transfer functions which express the relationship between the stresses and the sea state, Fig. 1.

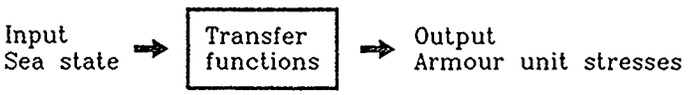

Fig. 1. Definition of stress transfer function.

The transfer functions are urgently needed. In order to stimulate the interest for research in this field the paper presents a more general discussion of the problems related to the determination of the stresses in slender types of armour units and the various tracks used so far. A more detailed description is given of a method based on combined model scale and prototype experiments, and specific results related to Dolosse are presented. The Dolos armour unit has been chosen because of its excellent hydraulic stability and because its structural strength can be adjusted by changing the waist ratio, i.e. the ratio of the shank diameter to the height of the units, see Fig. 2.

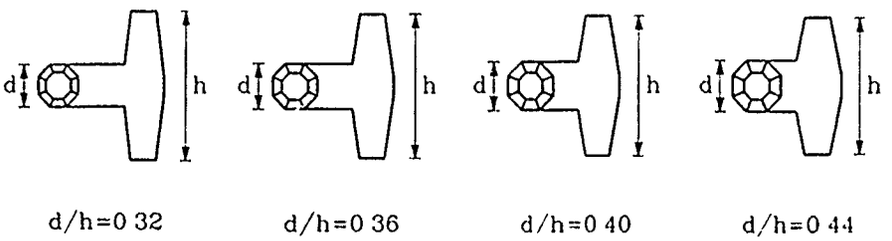

Fig. 2. Examples of Dolosse with different waist ratios but with equal mass.

By increasing the waist ratio to obtain larger strength the hydraulic stability will decrease somewhat, which must be taken into account in the design.

Overall procedure for the production and the use of design diagrams

Design diagrams are practical representations of the transfer functions, Fig. 1.

Due to the stochastic nature of the wave loads, the complex shape of the armour units and their random placement and orientation and consequently random structural support we are dealing with a problem which cannot be dealt with on a deterministic basis, but must be handled as a probabilistic problem.

The stochastic nature of the problem and the variety of the structural geometry and sea states, make it necessary to investigate a very large number of situations. This can be performed at reasonable costs only by small scale experiments with instrumented armour units, because no theory is available for quantative calculations, and large scale or prototype experiments are very expensive. However, all known types of small scale model experiments produce insufficient information about the armour unit stress distribution and involve scale and model effects of various kinds. For this reason the principal procedure must imply a checking and calibration of the behaviours of the small scale models against recorded prototype situations where no hydraulic and structural scale effects are present.

Thus the logic procedure will be as depicted in Fig. 3.

1. Prototype investigations of stresses in concrete armour units.
2. Small scale laboratory experiments of the investigated prototype breakwater covering the recorded prototype sea state situations.
3. Comparison of prototype and small scale results including the study of model effects and scale effects. Consequent calibration of the applied small scale laboratory experiment method.
4. Performance of a large number of small scale experiments comprising characteristic types of breakwaters for establishment of general design diagrams for stress response in armour units taking into account fatigue and other possible significant long term effects.

Fig. 3. Overall procedure for the establishment of design diagrams for structural integrity of armour units.

In the design process both diagrams or formulae for the hydraulic stability as well as for the structural integrity must of course be used together. Alternatively combined diagrams can be used.

Having established the design diagrams the design procedure is in principle as follows, Fig. 4.

1. Estimate the size of the armour units on the basis of requirements for hydraulic stability.
2. Determine the max allowable prototype stress, $\sigma_1^{critical}$ on the basis of the concrete tensile strength and the fatigue during the structural lifetime. Also consider a safety factor.
3. Scale σ_1 from transfer function (design) diagrams to obtain the prototype scale stress, $\sigma_1^{prototype}$. (Take into accont ratio of impact stresses to total stresses.)
4. If $\sigma_1^{prototype} > \sigma_1^{critical}$ change size or type of armour unit until the prototype stress does not exceed the critical stress.
5. Recheck the hydraulic behaviour of the armour layer If necessary go back to 1.

Fig. 4. Procedure for use of design diagrams for structural integrity of armour units.

Types of loads

The different types of loads on armour units and their origins might be listed as shown in Fig. 5.

TYPES OF LOADS		ORIGIN OF LOADS
STATIC		Weight of units
		Prestressing due to: Settlement of underlayers Wedge effect and arching due to movements under dynamic loads
DYNAMIC	Impact	Rocking/rolling of units Missiles of broken units Placing during construction } impacting solid bodies
	Pulsating	Gradually varying wave force including slamming Earthquake
ABRASION		Suspended material
THERMAL		Stresses due to temperature differences during hardening processes Freeze — thaw
CHEMICAL		Corrosion of reinforcement Sulfate reactions etc.

Fig. 5. Types and origin of loads on armour units (from Burcharth, 1981b).

Thermal and chemical loads will not be discussed in this paper. With respect to thermal stresses reference is made to Burcharth, 1983.

Impact loads used in this paper are defined as loads created by impinging solid bodies, i.e. armour unit against armour unit and armour unit against filter stones.

It is characteristic for both static and dynamic load conditions that a deterministic calculation of the stresses in the units is practically impossible, mainly because of the stochastic nature of the wave loads, the complex shape of armour units and their random placements.

It is also characteristic that these stresses do not scale the same way. Generally speaking the stresses due to non-impact loads increase linearly with the characteristic length of armour units, while impact-induced stress increases with the square root of the characteristic length. The relative importance of these stresses depends on the size and geometry of the units, their position on the slope and so on, cf. Fig. 6.

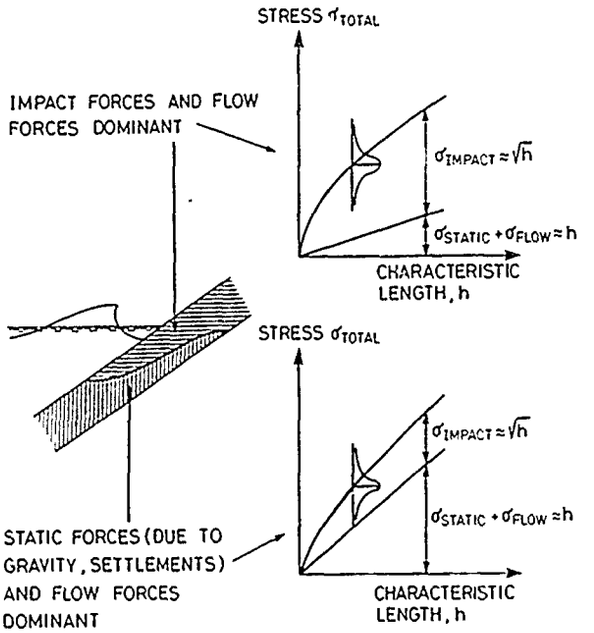

Fig. 6. Qualitative description of stresses in complex armour units as function of the size of units (from Burcharth, 1986). Note that ratio between σ_{impact} and $\sigma_{static} + \sigma_{flow}$ is very dependent on the design level. The ratio is small in case of a conservative design with very limited movements of the units

For this reason a correct conversion to another scale can be performed only if also the ratio between these two types of stresses is known. Consequently, the measured strain/stress signal must be analysed accordingly.

This is possible because the duration of an impact stress pulse is shorter by several orders of magnitude than a non-impact stress pulse. In principle a strain/stress signal must be analysed as shown in Fig. 7.

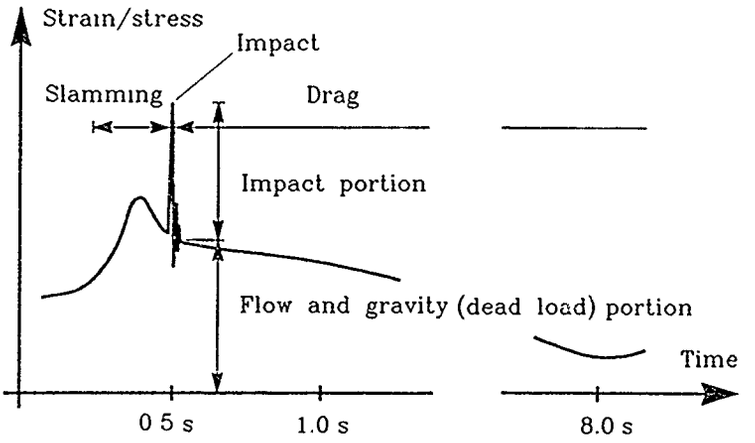

Fig. 7. Illustration of prototype strain signals comprising all types of strains/stresses (from Burcharth, 1988).

Fig. 8 illustrates the three regimes of Dolosse response measured from the 38 t prototype instrumented units at Crescent City.

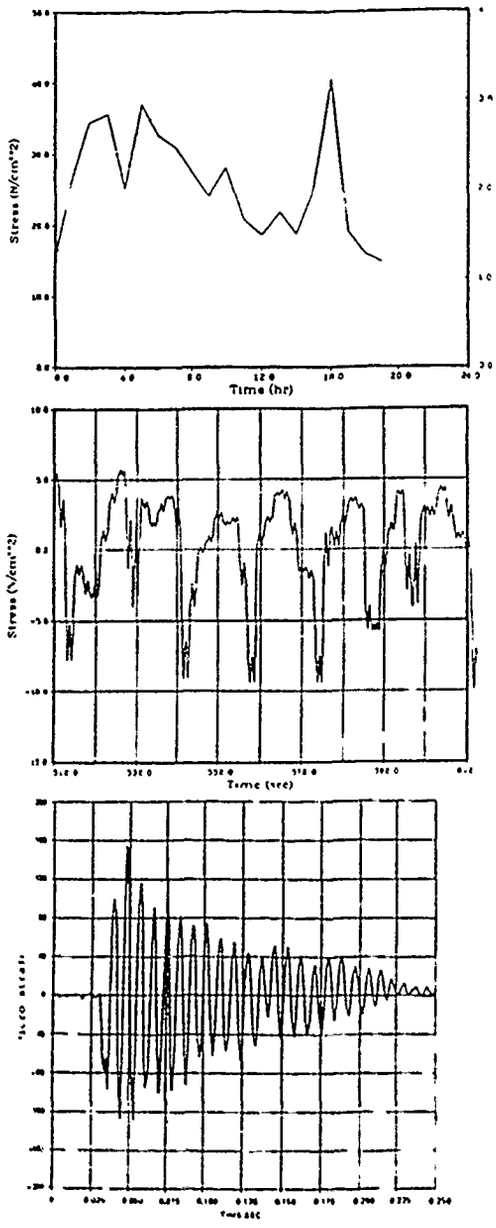

Fig. 8. Illustration of Dolosse response to static, pulsating, and impact loads, measured from 38 t instrumented units at Crescent City.

The first plot illustrates the static response due to the units self-weight and the interlock forces with surrounding units. The response can be seen to vary with tide over the 24 hour period. Moreover, a sudden shift in the stress level, probably due to a minor change in the position of the unit, is seen.

The second plot, which comprises 100 sec. of response history, illustrates the forces due to wave attack. The dominant wave period is app. 13 sec.

The third plot is the dynamic response in strain during a controlled drop test of the type shown in Fig. 9.

Methods of determination of stresses in armour units

Because of the recent dramatic failures of many large breakwaters throughout the world much attention has been paid to the assessment of armour unit structural integrity under wave attacks. Roughly speaking the research approaches can be divided into direct and indirect methods. The so-called direct method is the study of armour unit structural responses to wave attack by measuring or calculating the stresses in the units, while the indirect method implies the use of other charateristics instead of the stresses of the armour units.

Indirect methods

- Correct scaling of the most important material properties of concrete in small scale hydraulic model tests was first presented by NRC (Timco, 1981). However, it is impossible to correctly scale the material strength as the ratio between non-impact stresses and impact stresses is varying in the model and also unknown, as stated before. Moreover, no general information on stresses is obtained except the information on the exceedence of the strength level in case of breaking units.

- The armour unit movements under wave attacks can be estimated either by cine/video or by accelerometers installed inside the units (DHL, 1980; Howell, 1985; van der Meer et al., 1990). The idea of these methods is to get information about impact velocities on the basis of which impact loads and related stresses can be estimated by theoretical calculations. However, there are many problems. Cine/video techniques generally fail to give information in the splash zone and it is difficult to estimate size and direction of velocities from accelerometers. Moreover, it is almost impossible to arrive at good estimates on stresses from information only about movements of the impinging body unless we are dealing with a well defined system of solid bodies as was the case in a Dutch basic research study of impact generated stresses (Ligteringen et al., 1990). A less demanding approach is to evaluate the structural integrity by the comparison of the estimated and recorded impact velocities with critical impact velocities, i.e. velocities causing a specific amount of armour unit breakage for a certain unit and geometry of the structure. Such

critical impact velocities must be found either from theoretical calculations (which will be rather speculative), or from prototype recordings (which are extremely difficult and costly), or by relating model test results to known behaviour of prototypes. One of the main problems is that environmental and structural conditions for prototypes are very seldom well documented. Another problem is that the method only deals with stresses caused by impacts. Consequently, the static stresses and the pulsating stresses are not dealt with, but must be added theoretically, which is difficult, cf. the scaling problem explained in Fig. 6. Moreover, in case of large complex units the static stresses are expected to be rather dominant. Model test results presented in this paper and recordings from the 38 tons Crescent City Dolosse confirm this prediction (Melby et al., 1989).

- Based on the survey and data re-analysis of 10 Dolos breakwaters an energy method was presented by Timco, 1984, which checks whether the ratio of the incident wave energy to the size of Dolosse will exceed the critical one causing breakage. The method presents a rough estimate since no material characteristics enter into the formulae (Burcharth, 1983).

Direct methods

- A few years ago CERC started a large programme to acquire systematic measurements of structural kinematic and kinetic response of 20 instrumented 38 tons Dolosse, which were built and placed as part of the rehabilitation of the breakwater at Crescent City (Howell, 1985). Such systematic prototype measurements turned out to be a great success. Many contributions have been made, such as information on the magnitude and character of the static stress, the finding of a Rayleigh distribution for maximum principle tensile stresses due to waves in half an hour recordings for a given range of wave height in all boundary conditions and for all wave periods, the linear relationship between the maximum principle tensile stresses due to waves and the one-tenth wave height in half an hour recording (Howell 1988 and 1989; Melby et al., 1989). Some results from this research programme are presented and discussed in the present paper.

- With the purpose of establishing a relationship between size of units and impact stresses of unreinforced slender units, some full scale tests, namely drop tests and pendulum tests, of 1.5 tons to 30 tons Dolosse to destruction were performed by Burcharth, 1980. The set-up and the test procedure were proposed as a standard model for impact tests. Later on this test model has been followed by a number of researchers (e.g. Endo, 1985; Lin, 1986). The test results verify Burcharth's similarity-theory formulae for impact stresses, cf. Fig. 9.

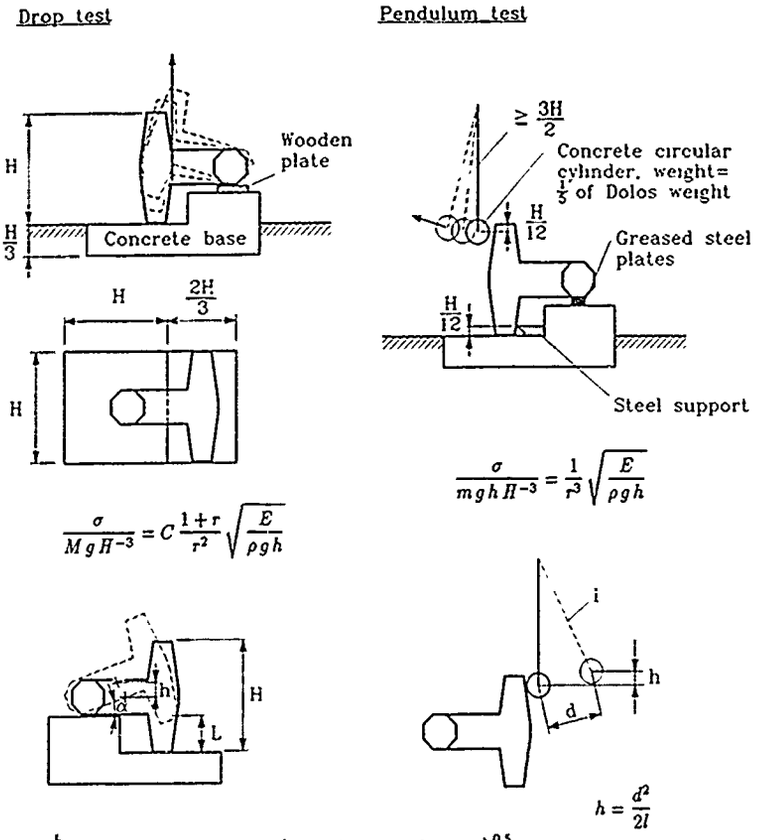

$$\frac{\sigma}{MgH^{-3}} = C\frac{1+r}{r^2}\sqrt{\frac{E}{\rho g h}} \qquad \frac{\sigma}{mghH^{-3}} = \frac{1}{r^3}\sqrt{\frac{E}{\rho g h}}$$

$$h = \frac{d^2}{2l}$$

$$\frac{h}{H} = [\sin(\alpha+\gamma) - \sin\gamma]\left(0.336r^2 - 0.293r^2 + 0.25\right)^{0.5}$$

$$\frac{L}{H} = [\sin\beta - \sin(\beta-\alpha)](1.118 - 0.943r)$$

$$\gamma = \sin^{-1}\left(\frac{r}{0.870}\right)$$

$$\beta = \tan^{-1}\left(\frac{1-r}{2-1.6r}\right)$$

C and K are constants.

Fig. 9. Impact test set-ups and corresponding formulae (from Burcharth, 1981(a) and 1981(b)).

- Photoelastic analysis used to obtain the static stress distribution inside armour units under the certain deterministic static loading conditions (Lillevang et al., 1976). It should be stressed that the photoelastic analysis can only be used for non-cracked concrete structures. When internal cracking occurs the stress analysis should be related to fracture mechanics theory, (Burcharth 1981(a)).

- Based on deterministic assumptions about loading conditions the stresses in slender armour units can also be determined by an analytical approach for example by use of numerical models (McDougal et al., 1988). However, at the moment such procedure only give qualitative information on this highly stochastic process.

- Strain gauge measurements at the surface of large model concrete armour units (50 kg Tetrapods) were performed by Nishigori et al., 1986. Considering the 50 kg concrete tetrapod as a model of a 50 tons prototype, prototype stresses of up to 2.9 MPa and 9 MPa for units rocking and rolling respectively were obtained. For comparison it can be mentioned that the ultimate tensile strength for conventional concrete of good quality is typically 4 MPa and 6 MPa for pulsating loads and impact loads respectively. However, since we are dealing with repeated loads, fatigue must be taken into account. Fig. 10 shows that even for a limited number of impacts the strength of conventional unreinforced concrete is reduced considerably.

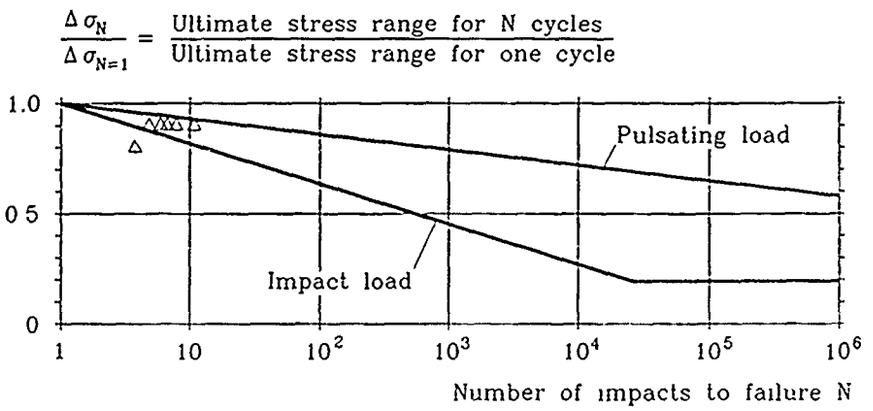

Fig. 10. Fatigue in conventional unreinforced concrete. Uniaxial and flexural stress (from Burcharth 1984). △ indicates results of Zwamborn et al., 1990, for semi-soft Dolosse impact tests. Note that the ultimate impact load strength for one cycle is app. 1.4 times the ultimate pulsating load strength, which can be taken equal to the static one.

The recorded impact stresses of 2.9 MPa as found for severely rocking 50 tons Tetrapods will in fact cause the units to break after app. one thousand impacts. Rolling will lead to immediate breakage (Burcharth, 1984 and 1987). Only the application of large scale model units, such as Nishigori's 50 kg Tetrapods, makes it possible to use strain gauges mounted directly on the surface of the unit. However, even in the case of 50 kg units it is difficult to obtain a reasonable signal due to the small strains related to static and pulsating loads. Moreover, the protection of the strain gauges is a problem because the length of the gauge must exceed the maximum size of the aggregates thus covering relatively large areas. In 1987 Burcharth tried surface mounted strain gauges on 200 kg Dolosse, but even for this large size of model armour units it was not possible to record static stresses with satisfactory accuracy. Consequently a load cell solution was adopted as mentioned below.

- As early as in 1974, strain gauges were placed on model units in the study of breakwater armour layers (Sandstrom, 1974). Strain gauge mounted load cells placed in Tetrapods to measure bending moments were used by DHL in 1980.

  Fig. 11 shows an example of an impact signal recorded by DHL.

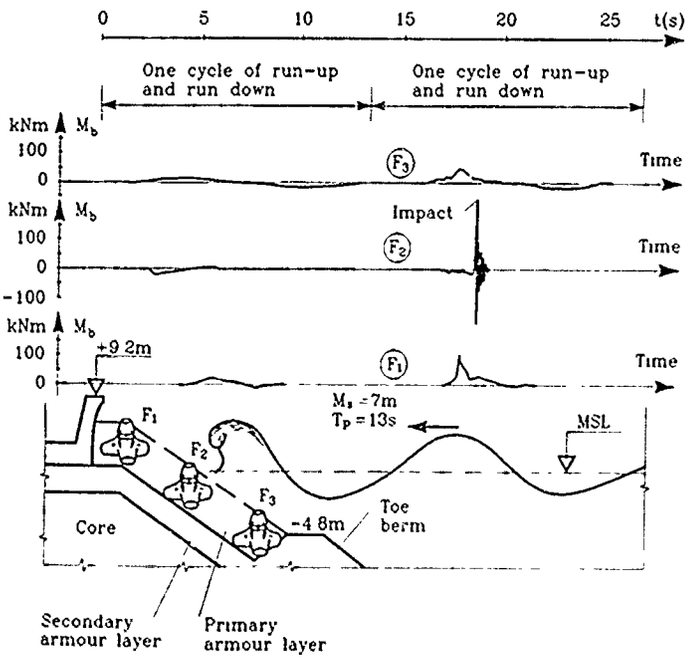

Fig. 11. Bending moments recorded in the legs of a Tetrapod (from DHL 1980).

Because slender armour units primarily experience bending and torsional moments due to the nature of their shapes, the axial and shear forces are considered to be of minor importance. An instrumentation method to measure only the bending and torsion moments by means of a load-cell inserted into one cross section of 428 g Dolosse was presented by Scott et al., 1986. The first generation load cells was installed at the mid-shank cross section and the stresses were transferred to the shank-fluke cross section of the Dolosse by applying a stress magnification factor. It was the consensus of the attendees of the 1985 Vicksburg Seminar on armour unit structural strength that the stress relationship between mid-shank and shank-fluke sections is not deterministic. Later on load-cell was installed also in the shank-fluke corner in static stress tests (Anglin et al., 1990). In 1988 CERC developed a very sensitive load cell able to record bending moments and torque in one shank-fluke section of 200 g model Dolosse (Markle, 1990). Some of these units were lent to University of Aalborg and the related test results together with results from tests with 200 kg Dolosse instrumented with load cells capable of measuring all component forces in 4 sections were presented in Burcharth et al., 1990. More results are included in the present paper. The most difficult problem to overcome when applying the load cell method is that impact signals cannot be correctly reproduced because the installation of the load-cell makes the material properties of the model units different from that of the prototype units. However, Burcharth et al., 1990, presented a way of overcoming this problem by impact calibration against prototype data from various impact tests with Dolosse of up to 20 t. The calibration analysis is presented in this paper.

Burger et al., 1990, performed large scale model flume tests with 50 kg Tetrapods instrumented in one cross section with a load cell able to measure the bending moment. The wave induced bending moment was studied and an impact calibration against monolitic Tetrapods of up to 1.8 t was performed.

Data reduction

Structural parameters:
The transfer functions, as defined in Fig. 1, are related to the geometry and the material characteristics of the breakwater elements, i.e. they depend on a large number of parameters. Since we do not have general formulae or theories which give the relationships, we must study the problem on an empirical basis by performing experiments. Because it is not possible to overcome a systematical variation of all parameters we can, first of all, restrict ourselves to simple types of armour layer geometries by leaving out multislopes and concrete cappings. Secondly we can retain only the most important parameters and finally try to group them in dimensionless parameters.

If we are dealing only with unreinforced slender types of armour units made of normal concrete and placed at random in a "normal" two layer system, we must as a minimum include the cross sectional parameters indicated in Fig. 12 together with the geometrical parameters describing the longitudinal properties (straight sections, bends, round heads).

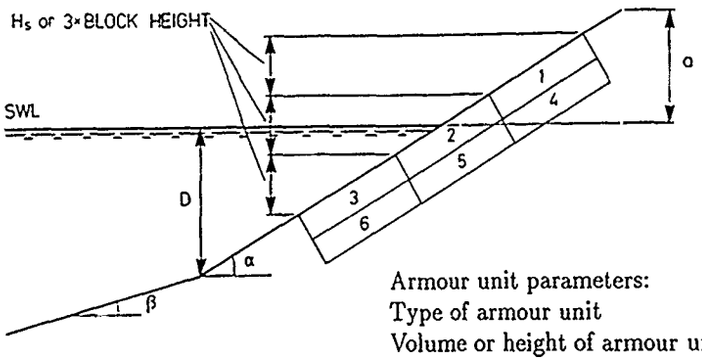

Armour unit parameters:
Type of armour unit
Volume or height of armour unit
Density of concrete
Elasticity or shock wave speed in concrete
Packing density
Position on slope (e.g. 1 - 6)
Under layer permeability/porosity coefficient
Settlement characteristics of sublayers

Fig. 12. Proposal for cross sectional and material structural parameters.

The parameters β (fore-shore slope) and D (depth at the toe) are more logically included/implemented in the sea state parameters and thus being excluded from the structural parameters.

As an alternative to the use of the significant wave height H_s as a measure for the extension of the six armour unit position areas, one could use a multiplum of the characteristic height h of the armour unit, e.g. $3 \cdot h$, cf. Fig. 2. In both cases the indicated part of the slope covers the area where the largest armour unit stresses will occur, provided that the armour units are resting on a conventional stone armour layer and not on a smooth under layer. In case of a smooth under layer one might expect large static stresses at positions lower than the areas 3 and 6.

Instead of keeping track of the unit position on the slope by dividing the slope into six areas (which is proposed to overcome the problem with upscaling of the stresses) one could for simplicity just use one area covering the same total portion of the slope. This will of course reduce the number of transfer functions to 1/6, but will also result in a larger scatter in the transfer function and somewhat reduced

possibilities for a rational transformation of stresses into other length scales in cases where impact generated stresses are significant.

In principle there will be a transfer function for each combination of the above given structural parameters if we cannot combine them in meaningful groups or delete those of minor importance.

Sea state parameters

The direction of the waves relative to the structure is an important parameter. The waves can be described either in the time domain by their height, H and period, T identified by the zero crossings of the surface elevation time series, or in the frequency domain by the variance spectrum, Fig. 13.

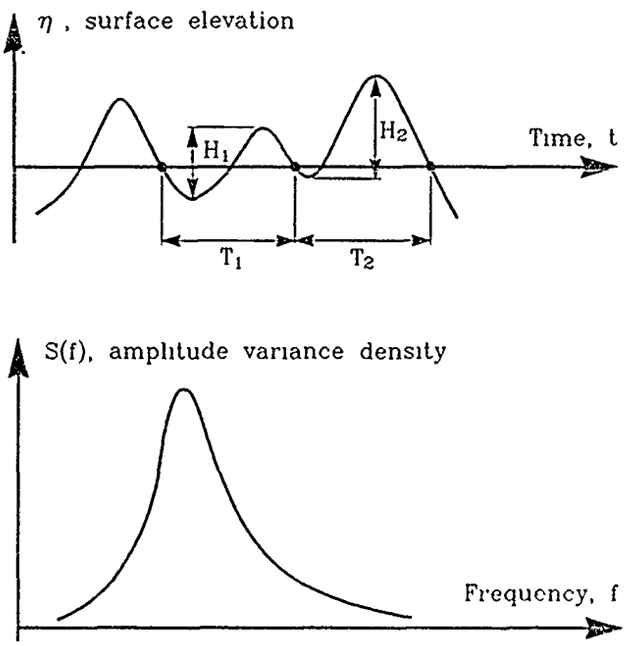

Fig. 13. Waves defined by the zero down crossings and by the variance spectrum.

Using the zero crossing definition of waves the down crossings are to be preferred because they define oncoming waveheights as seen from the structure.

The zero crossing definition makes it possible to perform a deterministic wave by wave response analysis, where each individual wave is related to the corresponding imposed stresses in the armour units. To apply this method simultaneous time series of waves and stresses are needed. To optimize the correlation between the

two signals the wave signal must be shifted in time corresponding to the average wave celerity times the distance from the wave gauge to the armour units.

The deterministic wave by wave reponse analysis is applicable only if the succession and the character (degree of instability) of the waves are more or less unchanged from the wave gauge to the toe of the structure. Generally these demands are fulfilled only in non-breaking wave situations (deeper water wave situations) with the wave gauge placed few wave lengths from the structure. Wave reflection will of course influence the wave train and blur the correlation to some extent, but this effect will be insignificant compared with the expected scatter in the analysis.

By performing a wave by wave analysis it is in fact assumed that the armour layer response is uniquely related to each separate wave defined solely by its H and T. Consequently the wave succession/wave grouping (the effect of the preceding wave) is not registered in the input, but it will of course be inherent in the output, cf. Fig. 1. This results in more scatter in the transfer function simply due to the fact that a specific wave defined by its H and T will impose different stresses in the armour units dependent on its position in the wave train.

In cases where the wave gauge is further away from the structure and/or the waves are shallow water waves involving a breaker zone in front of the structure a wave by wave analysis is not possible. Instead a time domain analysis can be performed where some characteristic upper values of the waves and the stresses are correlated, i.e. $H_{1/10}, \overline{T}$ and an upper fractile of the stress, i.e. $\sigma_{2\%}$.

Instead of characteristic wave parameters found from zero crossing analysis the spectral values can be used, as for example H_{m0} and T_p, in which case we are talking about a mixed time-frequency domain analysis.

A true frequency domain response analysis (Burcharth et al., 1988) uses the wave spectrum as input and the stress spectrum as output. The latter represents only the wave generated pulsating part of the stresses.

As to the wave spectrum it is assumed that we are dealing with random phases of component waves, i.e. the groupiness is determined by (inherent in) the shape of the spectrum and its position on the frequency axis. If we limit the general analysis to single peak spectra (omitting double peak spectra usually caused by combined swell and storm waves) it might be sufficient to characterize the spectrum solely by its characteristic values of heights and periods, e.g. H_s and T_p (or $T_{m,1}$) and subsequently relate the stress-response values to these parameters leaving out specification of the spectral shape. This proposal is supported by rock stability tests by Van der Meer et al. (1986) and run-up tests on armoured slopes by Allsop et al. (1985) where no significant influence of the type of spectra was found (Jonswap/Pierson-Moskowitz). Van der Meer used T_z as characteristic wave period whereas Allsop et al. used T_p.

The wave imposed loads on the armour units and the related stresses are determined by the kinematics of the wave which cannot be satisfactory described solely by the wave height and the wave periode or by the spectrum. In case of deeper water, i.e. situations where the waves in front of the structure are non-breaking, it is possible to characterize to some extent the kinematics of the wave action on

the breakwater slope by the surf-similarity parameter, ζ (also denoted the Irribarren number or the breaker parameter). This is because the various types of wave breaking on a slope correspond to specific ranges of ζ.

For a wave by wave analysis this parameter would be $\zeta = T\left(\frac{2\pi}{gH}\right)^{0.5} tan\alpha$, where α is the slope angle. In cases where the waves in front of the structure are described through the statistics of zero crossing waves or by the variance spectrum some characteristic values of wave height and wave period must be used, e.g. $\zeta = T_z\left(\frac{2\pi}{gH_{m0}}\right)^{0.5} tan\alpha$.

In case of shallow water situations with a breaker zone in front of the structure we have no single parameter which can characterize the kinematics of the waves in front of the structure and the wave action on the slope. For such cases one has to describe the foreshore sea bed profile together with either characteristic values of wave height and wave period (i.e. $\overline{H}, H_{1/3}, H_{1/10}, \overline{T}, T_{1/3}$) or the spectrum at some specific position (water depth) on the foreshore, preferably close to the structure. If for shallow water situations, only a deep water spectrum is available then a transformation of the spectrum to a shallow water position in front of the structure should be performed. The TMA shallow water spectrum might be used (Hughes, 1984).

Generally speaking it is a problem to describe in a relevant unambiguous way the sea state in front of a shallow water structure. Improvement on this matter will reduce the present large scatter we see in model test results for various types of response of breakwaters in shallow water.

Armour unit stress parameters

Only reinforced concrete armour units are considered in this paper.

When the tensile stress exceeds the tensile strength of the concrete a crack will be formed. The exceedence of the tensile strength is taken as the failure criterion although in most cases the body has some residual strength capacity after formation of the first cracks. Thus the failure criterion is

$$\sigma_1 > S$$

where σ_1 is the *maximum principal tensile stress* occurring in the body and S is the tensile strength of the concrete. The failure criterion is discussed in Appendix A.

The output of the response analysis should then be σ_1.

In the case of wave by wave response analysis the parameter value of the stress should be "the maximum peak value" within each wave period.

In the case of a response analysis in the frequency domain we must obtain a stress power spectrum based on a continuous signal of the variation of σ_1 with time.

The basis for the calculation of σ_1 will be strain measurements in instrumented sections of the armour units, cf. the discussion of the various methods earlier in the paper.

Other sections than the instrumented one(s) might experience larger stresses. For such sections estimates on σ_1 might be produced by means of finite element analysis simulations. However, this is very difficult for which reason it is very important to select the most critical section(s) for load cell instrumentation.

As explained various types of forces contribute to the stress σ_1. Unfortunately stresses generated by impact forces scale differently from gravity and flow force generated stresses. Consequently the component stresses (or forces) should be scaled correctly before being added to form the total stresses.

Because the maximum stresses generated by the various types of forces do not occur in the same point within a cross section of the armour unit one has in principle to determine the component stresses over the entire cross section in question, then add them and finally extract the maximum value. Such a procedure involves a lot of computation. An easier approach would be to determine the cross section force components (bending moments M_y, M_z, torque, T, shear forces V_y, V_z and axial force, N_x) for each type of loads, convert them to prototype scale, add them and then calculate the maximum principle tensile stress, σ_1. Appendix A explains the calculation of σ_1 for instrumented cross sections of a Dolos.

The ultra short duration of impact loads makes it necessary not only to sample data with a very high frequency but also to perform a large number of stress calculations densily spaced in the time to ensure identification of the stress peak value.

The required sample frequency to capture sampling stresses can be estimated from dynamic modal analysis of the armour unit shape. Modal analysis may be performed either analytically, using simplified beam representations, or using the Finite Element Method (FEM) with a more accurate representation of the structure, or experimentally using spectral analysis of measured dynamic accelerations when the structure is subjected to a test impact. The distribution and relative magnitude of the modes vary according to boundary conditions and the submergence depth of the unit. All three methods have been applied to the dolos unit (Hall et al., 1986). Tests were performed on 1.8 ton and 38 ton dolosse units. The natural frequency of the first mode for 38 ton units was found to be 115 Hz. For the 200 g load cell instrumented CERC Dolosse it is app. 1000 Hz (Burcharth et al., 1990). The measurement system should have adequate bandwidth, F_{bw}, to capture the highest mode of interest. Assuming proper input filtering to prevent aliasing, reconstruction filters may be used during postprocessing to reproduce impact waveforms. The minimum required sampling frequency is

$$F_s = 4\, F_{bw}$$

It is important to note that the measurement equipment and input filters must maintain good linear phase response so that the shapes of high rise time stress signals are not distorted.

Convertion of impact stresses found in load cell instrumented units to the corresponding stresses in homogeneous monolitic prototype units constitutes a special problem which is dealt with later in the paper.

Also from a computational point of view it is a great complication that impact induced stresses have to be separated from the total stresses, cf. Fig. 7. In the case of a response analysis in the frequency domain, i.e. the transfer function is obtained from a continuous wave amplitude signal and a continuous principal stress signal, it is necessary to separate the impact induced stresses. This might be accomplished by recognizing that the time scales of the stresses are different. Combined impact and flow generated stresses may be separated by a digital low pass filter followed by time decimation of the input data to obtain the flow stresses, and by trend removal to isolate the impact stresses.

So far the wave by wave response analysis has shown that in case of Dolosse it will be reasonable to separate the armour response in the following two categories:

1. Units not moving and not being exposed to significant impacts from other units, i.e. no significant impact generated stresses.

   This situation is predominant not only for units situated in the armour bottom-layer but also for the top layer units provided that a somewhat conservative hydraulic design criteria with very limited movements of the units is applied. This holds for even smaller size of prototype Dolosse. Thus the linear scaling of stress with the length scale can be applied and will be on the safe side if possible impact generated stress contributions are recorded and treated as static and pulsating stresses.

2. Units rocking and being displaced.

   Such units are predominantly sitting in the top layer. Impact generated stresses will be a dominant part of the total stresses and can be treated in accordance with the non-linear scaling law. Because this scaling law is on the unsafe side if flow and gravity generated stresses of any significance are present an estimated correction might be performed or alternatively a modified scaling law applied. This situation is relevant to units which are being impacted by moving units.

Dolos static stress experiments in the dry (ramp tests)

Description of the experiment

With the purpose of studying the characteristics of static stresses in Dolosse and the related model and scale effects, a large on land experiment programme was started in 1986 in Aalborg Hydraulic Laboratory (AHL) at Aalborg University. It includes comparative compaction experiments with 200 kg and 200 g Dolosse placed on ramps with various slope angles. The geometries of the Dolosse are given in Fig. 14.

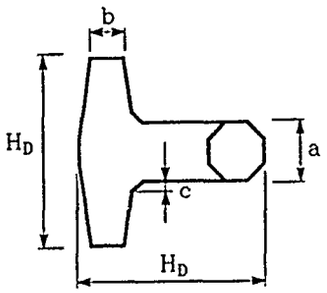

	app. 200 kg	app. 200 g
height H_D (cm)	80	8
waist width a (cm)	26	2.6
head width b (cm)	16	1.6
height of fillet c (cm)	4 0	0 46
waist ratio	0.325	0 320

Fig. 14. Geometry of Dolosse.

To demonstrate the influence of the armour unit surface roughness on the static stresses, two materials were used for the 200 g unit, namely bronzefilled polyester (smooth surface) and concrete mortar (rough surface). The 200 kg units were made of ordinary concrete.

200 kg strain-gauged Dolosse

Based on the structural consideration and practical experience, it is now generally accepted that Dolos fractures tend to occur in or near the shank-fluke interfaces. Consequently, two shank and two leg cross sections near the shank-fluke interfaces of 200 kg Dolosse were chosen as strain-gauged sections. Because the signals from the surface mounted strain gauges turned out to be too weak, a load cell solution was adopted. Four strain-gauge rossettes were mounted on the surfaces of steel tubes inserted as load cells in each of the chosen sections, cf. Fig. 15.

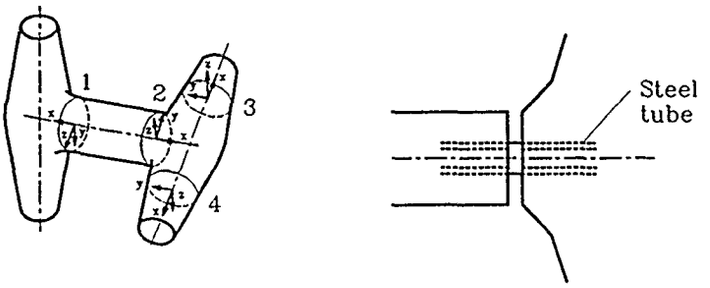

Fig. 15. Instrumented sections. 200 kg concrete Dolosse, Aalborg Hydraulic Laboratory (AHL).

The load cells allowed the following component forces/moments to be recorded, cf. Fig. 16.

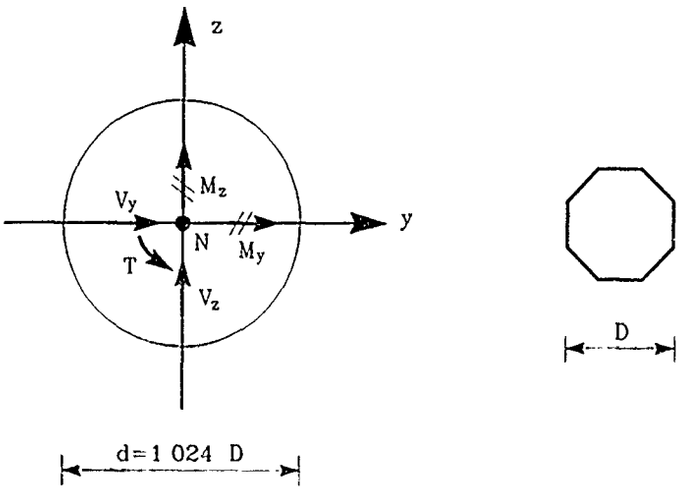

Normal force	N
Torque	T
Bending moments	M_z , M_y
Shear forces	V_z , V_y

Fig. 16. Component forces/moments recorded in the instrumented sections.

The instrumentation made it possible to verify the relative importance of shear and axial forces.

200 g strain-gauged Dolosse

The applied units are developed by CERC and lent to University of Aalborg (Markle, 1990). One shank cross section in the shank-fluke corner was strain-gauged to obtain two orthogonal bending moments and the torque. The stress contributions from axial and shear forces, which were believed to be of minor importance, were neglected.

The applied signal analysis, i.e. the transformation of the recorded load cell strains to armour unit stresses, is described in Burcharth et al., 1988. The first step of the signal analysis is to calculate the component forces/moments in the steel tube sections according to the recordings of strains. The next step is to transform these component forces into the stresses in the corresponding Dolos sections, and finally to calculate the maximum principle tensile stress, which is chosen as the critical parameter for the structural integrity of the armour units.

A large ramp (5 x 4 m) and a small ramp (0.5 x 0.4 m) with changeable slope angles were built. 72 Dolosse (200 kg or 200 g), including the instrumented ones, were randomly placed in two layers on the ramp. Every experiment involved the following 4 steps and corresponding recordings.

(i) Zeroing of strain gauges while the two instrumented Dolosse were in specified position resting unloaded on ground.
(ii) Placement of the Dolosse on the ramp.
(iii) Vibration of the ramp.
(iv) Removal of Dolosse from the ramp and placement of the two instrumented Dolosse in the position described under (i).

Three pre-determined slopes were used: 1 : 0.9, 1 : 1.38 and 1 : 2. The instrumented Dolosse were 'randomly' put at positions 1 and 2 in the bottom layer, as shown in Fig. 17.

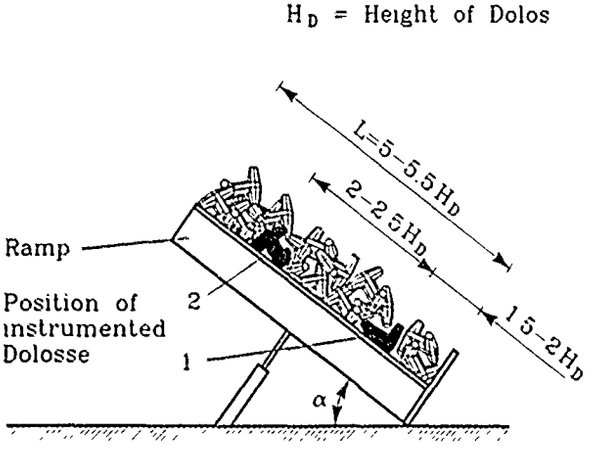

Fig. 17. Dolos compaction experiment set-up (AHL).

Results from the static stress experiments (ramp tests)

Comparison of stresses in the shank and fluke cross sections

Because the small scale units cannot for practical reasons be instrumented in the fluke sections it is important to investigate if this implies a model error of any significance. From the tests with the 200 kg Dolosse it is clearly demonstrated in Table 1 that the max principle tensile stresses in the shank cross sections generally are bigger than those in the fluke cross sections.

Table 1. 200 kg Dolos compaction experiment results.

Group	1	2	3	4
Slope	1 : 0.9	1 : 1.38	1 : 1.38	1 : 2
Instrumented Dolos position	1	1	2	1
σ_T in shank (MPa) Average μ_{σ_T}	0.336	0.167	0.151	0.166
μ_{σ_T} in fluke (MPa) Average μ_{σ_T}	0.181	0.157	0.088	0.12
No. of tests	28	40	36	20

σ_T denotes the max principle tensile stress in strain-gauged sections.

It is also seen that when dealing with results based on stresses only measured in the shank section it is necessary to compensate for the influence of fluke failures.

If it is assumed that the only relevant failure modes are fracture in the type of sections shown in Fig. 15, i.e. 2 shank sections and 4 fluke sections, then it is possible to calculate the probability of failure for the Dolosse, P_{Dolos}, from the probability of failure in the fluke section, P_{fluke}, and the probability of failure in the shank section, P_{shank} if the correlations between the various failure modes are known. If the Dolos is modelled as a series system, consisting of n elements $i = 1, 2, \ldots, n$, i.e. the failure of the Dolos takes place when only one of the element fails, then the probability of failure for the Dolos can be estimated as

$$P_{Dolos}(\sigma_T) \simeq 1 - \Phi_n(\bar{\beta}; \bar{\bar{\rho}})$$

where $\bar{\beta} = (\beta_1, \ldots, \beta_n)$ and $\beta_i(\sigma_T) = -\Phi^{-1}(P_i(\sigma_T))$ is the generalized reliability index corresponding to failure mode i. Each failure mode is approximated by a linear failure function in independent standard normal variables.

$\bar{\bar{\rho}} = [\rho_{ij}]$ is the correlation matrix for the linear failure functions.

Φ_n = n-dimensional standardized normal distribution.

Calculation of $\Phi_n(\bar{\beta};\bar{\bar{\rho}})$ for $n \geq 3$ cannot be performed exactly but the Hohenbichler approximation can be used (Thoft-Christensen et al. 1986). $n = 6$ in the proposed model for a Dolos. Alternatively reliability bounds can be calculated. A simple lower bound is the maximum probability of failure of any element, in this case corresponding to P_{fluke}. This lower bound corresponds to full correlation between all elements, i.e. $\rho_{ij} = 1$ for all i and j. A simple upper bound can be found by assuming non-correlated elements in which case we get

$$P_{Dolos}(\sigma_T) = 1 - (1 - P_{shank}(\sigma_T))^2 (1 - P_{fluke}(\sigma_T))^4$$

The assumption of non-correlated elements gives the highest possible probability of failure. More narrow bounds can be found if the correlations are known. The simple lower and upper bounds are shown in Fig. 19.

The correlations between the stresses in the shank and the fluke sections are presently under investigation.

Influence of Dolos position and slope angle

The results in Table 1 show as expected that the dolosse situated in lower positions of the bottom layer have greater stresses than those situated in the higher positions, and the dolos stress increases with steeper slopes, other conditions being equal.

The stress distribution

The measured maximum principal tensile stresses σ_T followed the log-normal distribution both in the shank and the fluke cross sections. The density function is given by

$$f(\ln \sigma_T) = \frac{1}{\sigma\sqrt{2\pi}} e^{-\frac{1}{2}\left(\frac{\ln \sigma_T - \mu}{\sigma}\right)^2}$$

$$\mu = \frac{1}{N}\sum_{i=1}^{N} \ln(\sigma_T)_i \qquad \sigma^2 = \frac{1}{N-1}\sum_{i=1}^{N} (\ln(\sigma_T)_i - \mu)^2$$

where μ and σ are average and standard deviation respectively.

Fig. 18 shows examples of the stress distribution in the shank cross section at the fluke-shank interface. The influence of shear and axial forces are included in the results from the 200 kg Dolosse but are neglected in the results from the 200 g units.

The conclusion on stress distribution is consistent with results from small scale tests conducted by D. Turke, Canada (private communication), see also Anglin et al., 1990.

200 kg Dolosse

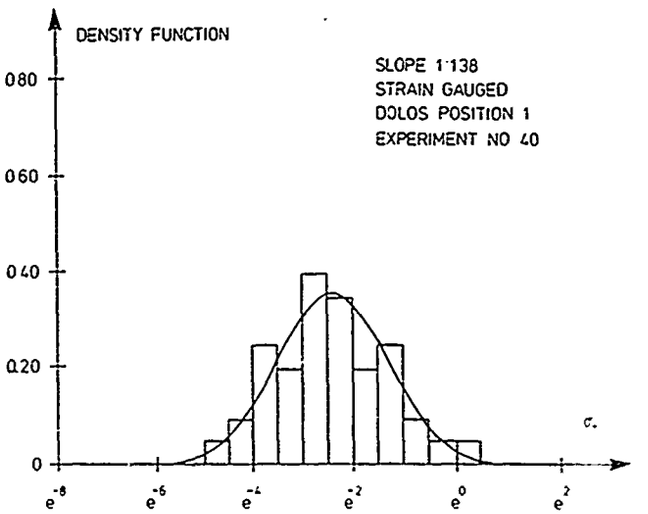

200 g bronze filled polyester Dolosse

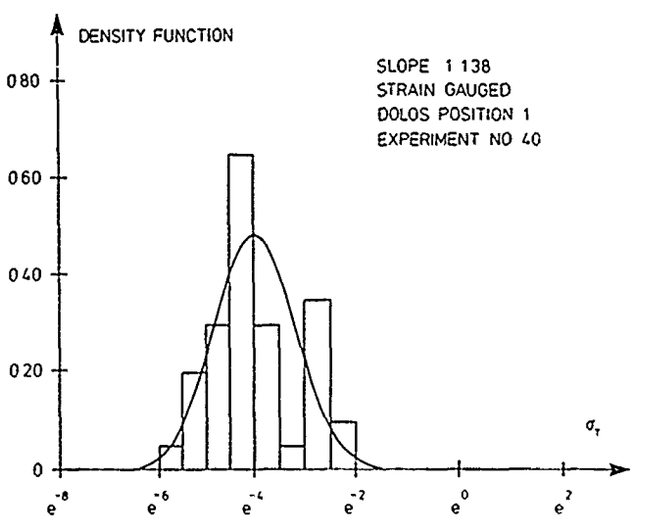

Fig. 18. Stress distribution in the shank cross section at the fluke-shank interface, AHL experiments.

Fig. 19 is an illustration of the influence of the six failure modes discussed earlier under the assumption of no-correlation.

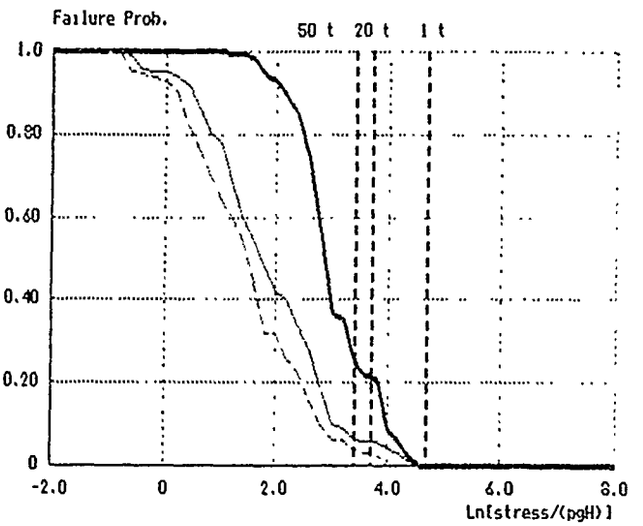

Simple upper bound of Dolos failure probability
(assuming no correlation of failures in flukes and shanks)

Failure probability of shank
(Simple lower bound of Dolos failure probability)

Failure probability of fluke

Structural limitation of Dolosse with
weight 1, 20 and 50 t
waist ratio 0.32
density 2300 kg/mXX3
strength 3.5 MPa

Results from 200 kg Dolos ramp tests, axial and shear forces included

Instrumented Dolos positions 1 and 2

Slope of ramp 1:0.9, 1:1.33 and 1:2

Sample size 124 stresses in shank and fluke sections respectively

Fig. 19. Failure probability of Dolosse based on recorded static stresses in ramp tests in the dry, AHL experiments.

Stress contribution from shear and axial forces

In small scale tests it is difficult or even impossible to mound a sufficient number of strain gauges inside small Dolosse to determine all component forces/moments in a cross section. Generally the stress contributions from axial and shear forces are regarded of minor importance. To check this hypothesis the distribution of $(\sigma_T - \sigma'_T/\sigma_T)$, where σ'_T represents the corresponding maximum principal tensile stress without axial and shear forces, is plotted in Fig. 20. The results are from the fully instrumented 200 kg Dolosse and represent only the conditions in the instrumented shank sections. From this Figure the following can be concluded:

(i) the bigger σ_T, the smaller $(\sigma_T - \sigma'_T/\sigma_T)$, i.e. reduced influence from axial and shear forces.

(ii) The negligence of axial and shear forces most likely results in overestimation of the max principal stress. In other words, it is on the safe side.

Slope : 1 in 0.9, 1.38, 2. Instrumented Dolos position 1, 2
- - - : Fracture limitation of concrete Dolosse
(density 2300 kg/m^3, tensile strength 3.5 MPa)
— · — : Exceedence probability

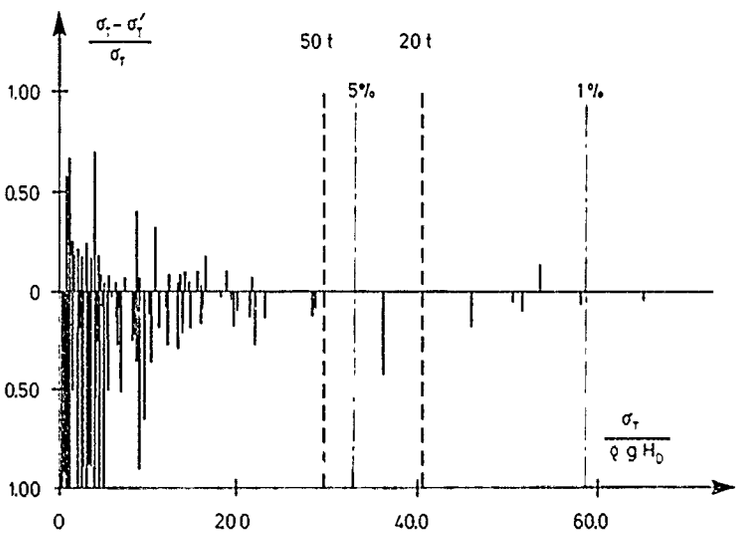

Fig. 20. Example of stress contribution from axial and shear forces. Tests with 200 kg Dolosse, AHL experiments.

Influence of compaction intensity and surface roughness

It is well-known that during the early life of a breakwater the armour units settle in moderate wave climates. Prior to armour unit layer stability tests the models will usually be exposed to a fairly large number of waves sufficient to cause some settlement/compaction of the armour layer without causing damages. Intuitively such compaction will cause the armour units to be more interlocked, and consequently increase the hydraulic stability of the armour layer. At the same time the stresses inside the Dolosse will increase due to the wedge effect, which again increases with the surface smoothness of the units. To demonstrate this, experiments were done with different compaction intensity, for smooth Dolosse (made of polyester, density is 2400 kg/m) and rough Dolosse (made of concrete, density is 2300 kg/m). The results, which are shown in Fig. 21, can be summarized as follows: The larger the compaction/settlement and the smoother the surface roughness the bigger the tensile stresses. The effects are of such significance that they should be considered in model test analyses.

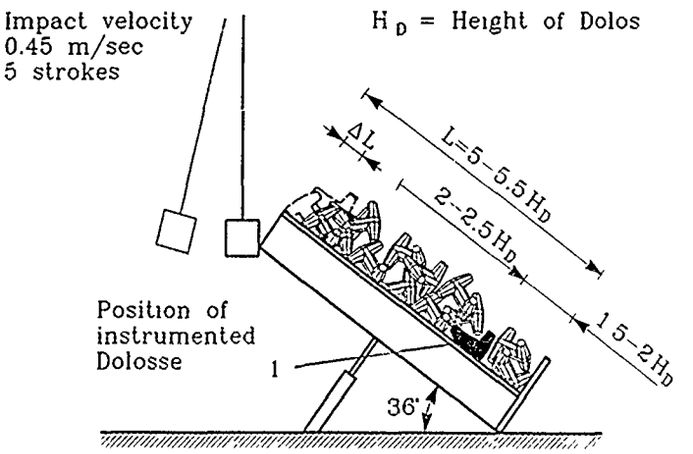

compacting weight in kg	Average of σ_T (MPa) in shank cross section of smooth units (polyester)	rough units (concrete)
1	0.031	0.022
2	0.033	0.026
3	0.039	0.028

Fig. 21. Influence of layer settlement on Dolos stress (results are not corrected for the small difference in armour unit densities).

Fig. 22 shows an illustration of the effect of surface roughness on the stresses in the armour units.

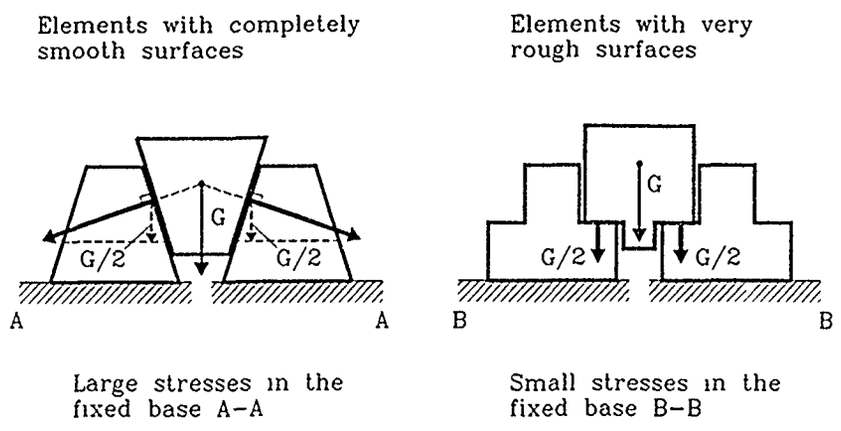

Fig. 22. Illustration of the effect of surface roughness on the stresses in the armour units.

Comparison of static stress distributions in large and small scale experiments including verification of the scaling law

Fig. 23 shows the exceedence probability of the dimensionless principle tensile stress in 200 kg and 200 g concrete Dolosse in the compaction experiment. It is consistent (especially for high stress levels), with the theoretical scaling law $\lambda_\sigma = \lambda_\rho \lambda_L$, where $\lambda_\sigma, \lambda_L$ and λ_ρ are scaling factors for stress, length and density, respectively.

Slope : 1 in 0.9, 1.38, 2. Instrumented Dolos position: 1 and 2.
--- : Fracture limitation of concrete Dolosse (density 2300 kg/m^3, tensile strength 3.5 MPa)
--- : 200 g concrete Dolos (without shear and axial forces)
--- : 200 kg concrete Dolos (without shear and axial forces)

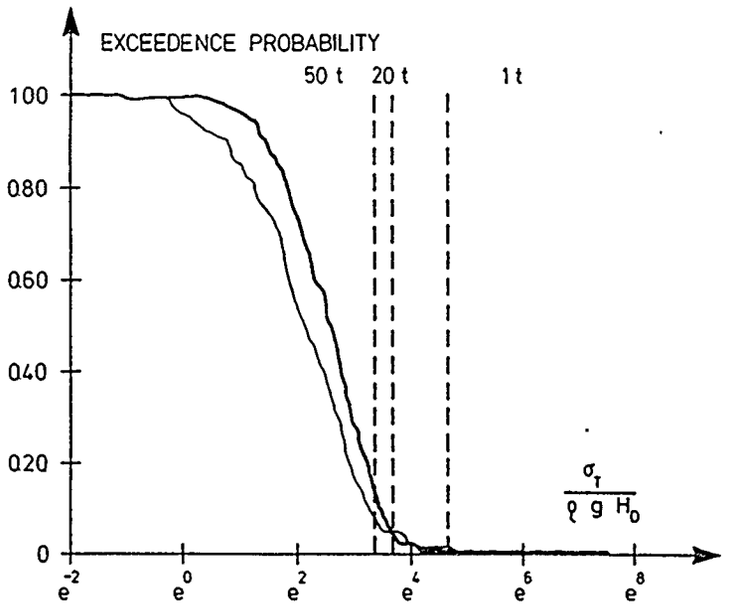

Fig. 23. Comparison of stress distributions in shank cross sections of 200 kg and 200 g concrete Dolosse armour. Influence from shear and axial forces are neglected. AHL experiments.

Hydraulic flume tests

The objective of the flume tests at AHL is to study the armour unit stresses as functions of the structural and the sea state parameters.

Although a comprehensive parametric study has not yet been completed, enough tests have been made to present some conclusions related to a range of problems. The set-up and procedure for the tests are coordinated with tests at CERC, Vicksburg, in order to establish a more complete parametric study.

Model test set-up and description of the experiments

All tests were conducted in a 1.2 m wide and 1.5 m deep flume with the model situated app. 17 m from the wave paddle, Fig. 24. The flume was divided into two parts with widths of 0.75 m and 0.45 m, respectively. The breakwater model was placed in the 0.75 m wide part of the flume at the top end of a 1 : 20 foreshore slope. The water depth at the toe of the breakwater was 23 cm. The 0.45 m wide part of the flume was fitted with an effective non-reflecting array of perforated metal sheets.

To compensate for reflected waves two arrays of three wave gauges were installed. The incident wave spectrum was calculated by the least square method presented by Mansard et al., 1980.

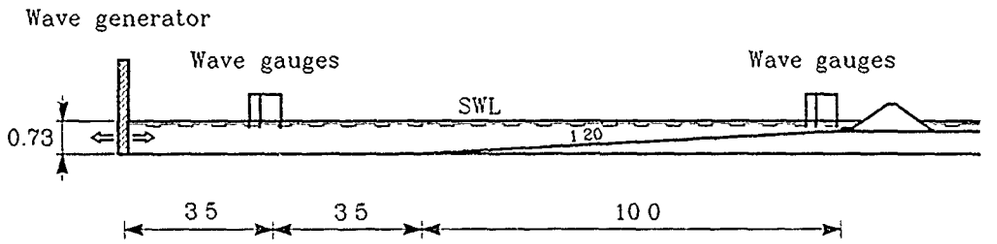

Set-up of the wave flume

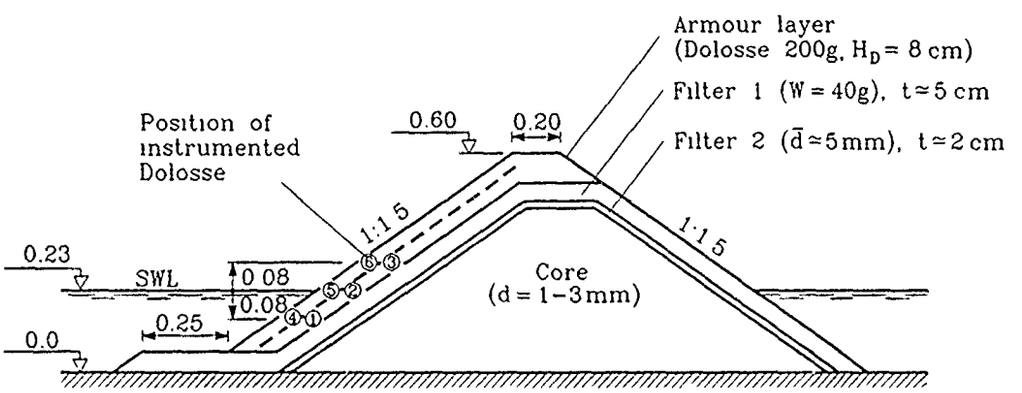

Cross section of the breakwater

Measures and levels in meter

Fig. 24. Set-up of the wave flume and the cross section of the breakwater. AHL experiments.

The irregular waves were generated by a piston type paddle according to the five parameter JONSWAP spectrum.

$$S(f) = \alpha H_s^2 T_p^{-4} f^{-5} exp\left[-1.25\left(\frac{f}{f_p}\right)^{-4}\right] r^{exp\left[-\frac{\left(\frac{f}{f_p}\right)^2}{2\sigma^2}\right]}$$

in which

$$\sigma = \frac{0.0624}{0.23 + 0.036r - 0.185(1.9 + r)^{-1}}$$

$$\sigma = 0.07 \quad \text{for} \quad f < f_p$$

$$\sigma = 0.09 \quad \text{for} \quad f > f_p$$

and the peak enhancement coefficient r is 4.

Table 2 lists the characteristics of the applied waves propagating towards the breakwater at the paddle and at the toe of the breakwater. L_p is wave length corresponding to the spectral peak period and $\zeta = T_p \left(\frac{2\pi}{gH_{m0}}\right)^{0.5} tan\alpha$.

Table 2. H_{m0} and T_p at the wave paddle and at the toe of the structure.

H_{m0}^p	at the paddle	(cm)	5	10	15
T_p	at the paddle	(sec)	1.5	2	2
H_{m0}/L_p	at the paddle		0.016	0.022	0.032
H_{m0}^t	at the toe	(cm)	5.7	11.8	17.9
T_p	at the toe	(sec)	1.5	2	2
ζ	with H_{m0}^p and $tan\alpha = \frac{1}{20}$		0.27	0.25	0.21
ζ	with H_{m0}^t and $tan\alpha = \frac{1}{1.5}$		3.3	3.1	2.5

The cross section of the breakwater is shown in Fig. 24. The crest level was chosen such that no overtopping took place within the applied range of sea states.

The armour consisted of 200 g bronze filled polyester Dolosse with a waist ratio of 0.32 and mass density of 2.32 t/m^3. A two-layer system with a packing density of 0.74 and random placement of the units was applied. The instrumented units (see Markle, 1990) were placed in six positions, 1-6 shown in Fig. 24. The vertical spacing of 8 cm corresponds to the height, H_D of the units. The 5 cm thick primary filter layer was made of crushed stones with average mass of 40 g, i.e. 20% of the Dolosse mass. The 2 cm thick secondary filter was made of crushed

stones with diameters in the range 0.4 to 0.6 cm. The core consisted of sharp sand with diameters of 0.1 to 0.3 cm.

The test procedure was as follows

1. Calibration of the load cell instrumented Dolosse.
2. Zeroing of the strain gauges of the instrumented Dolosse while placed in a zero-load position
3. Placement of all Dolosse, including the instrumented ones on the slope.
4. Recording of strains.
5. Run of sea state corresponding to $H_{m0}^{p} = 5$ cm for 5 minutes (150-200 waves) while sampling strains at 20 Hz.
6. Recording of strains after the water table became tranquil.
7. Repeat steps 5 and 6 with sea states corresponding to $H_{m0}^{p} = 10$ cm and 15 cm.
8. Repeat step 2 and check possible zero drifting.

This procedure was repeated 20 times, i.e. the number of runs were 20 for each sea state and each position of the instrumented Dolosse.

Methods of analysis of the maximum tensile stress time series

The time series of the maximum principal tensile stress σ_1, at the surface boundary of the instrumented cross section are computed from the measured bending moments and torque, cf. Appendix A. Note that σ_1 is a function not only of the time, but also of the location on the surface boundary, i.e. the point where σ_1 occurs varies with time.

This makes separation of the static and pulsating stresses from the σ_1-signal complicated and introduces two definitions of the static stress as can be explained by the following simple example:

Assume a cross section exposed only to a static moment plus a harmonic oscillatory bending moment, Fig. 25.

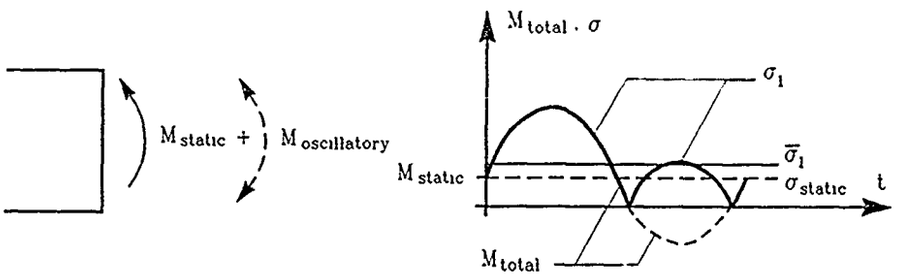

Fig. 25. Illustration of difference between the static maximum principal tensile stress and time average of the maximum principal tensile stress.

It is seen that the static maximum principal tensile stress, σ_{static} which is generated only by the static moment will be different from a static stress defined as the time average of the maximum principal tensile stress, $\bar{\sigma}_1$, the latter being the larger one. In general $\bar{\sigma}_1$ is different from σ_{static} but the difference is small and negligible in case of dominant static stresses. This is for example the case for the 38 t Crescent City Prototype Dolosse.

σ_{static} can always be determined from the averages of the recorded component forces (bending moments, torque, shear and axial forces) provided we are dealing with a stationary situation with no changes in the static stress. However, very often there are changes (shifts, trends) in the static stresses during a stationary sea state in which case σ_{static} will be an average figure for the recorded period. In case of model studies σ_{static} can be determined for the situations before and after the wave action, and an average value applied.

Fig. 26 shows a comparison between the two definitions of static stresses based on the model tests with the 200 g Dolosse.

Dolos position	H_s cm / σ_{static} MPa / $\bar{\sigma}_1$	5	10	15
1		0.015 / 0.015	0.016 / 0.016	0.017 / 0.017
2		0.017 / 0.019	0.016 / 0.019	0.016 / 0.019
3		0.014 / 0.016	0.017 / 0.017	0.018 / 0.021
4		0.009 / 0.01	0.009 / 0.01	0.01 / 0.011
5		0.012 / 0.015	0.013 / 0.015	0.012 / 0.016
6		0.006 / 0.009	0.007 / 0.009	0.008 / 0.008

σ_{static} = average of maximum principal tensile stresses before and after exposure to waves. Mean of 20 tests with replacement of the Dolosse.

$\bar{\sigma}_1$ = average of maximum tensile stress during 5 minutes stationary sea states. Mean of 20 tests with replacement of the Dolosse.

Fig. 26. Comparison of applied definitions of static stress in Dolosse. (The position of the Dolosse is shown in Fig. 24.) AHL experiments.

It is seen that for Dolos position 1 for which the static stresses are rather dominant (cf. Fig. 32) the difference is negligible (within 5%). For Dolos positions 3 and 6 where the pulsating stresses are more dominant the deviations are in the range 15-50%. As an average for all tested positions the deviation which is one sided is app. 15%.

Method of definition of peaks of static plus pulsating stresses

Fig. 27 shows an example of a time series of the maximum principal tensile stress, σ_1 for a 200 g Dolos which is not exposed to impacts in the flume tests, i.e. only static and pulsating forces are acting.

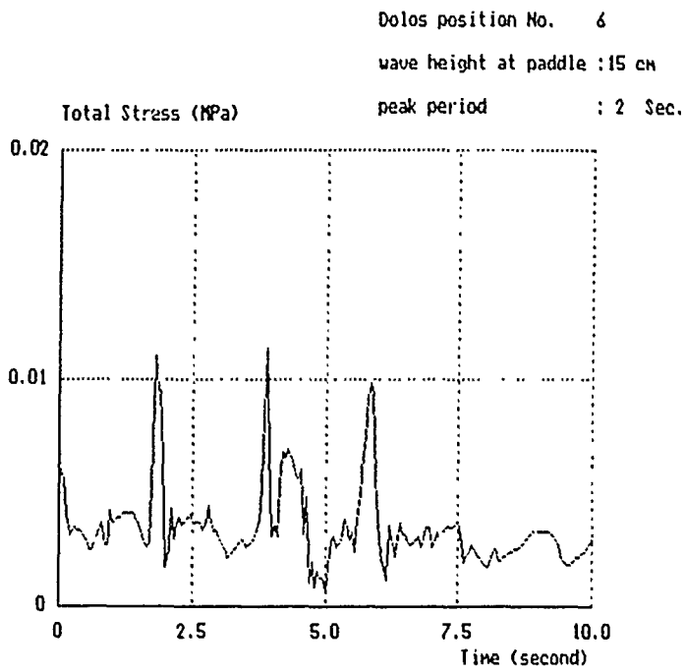

Fig. 27. Time series of static plus pulsating maximum principal tensile stress in a 200 g instrumented Dolos. AHL experiments.

In the statistical analyses of the stress peaks presented in the paper a definition of the peaks by zero down crossing identification has been adopted, Fig. 28.

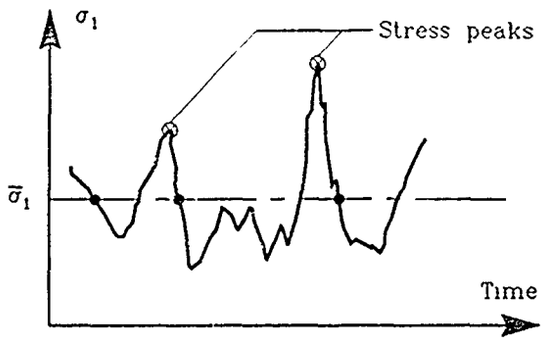

Fig. 28. Definition of peaks of stress in time series.

Correction for multi failure modes of the Dolos

As discussed earlier and illustrated in Fig. 19 the results based on stress records from a single cross section should be corrected to take into account other possible failure modes.

Unfortunately, no prototype studies or model flume tests performed so far involve simultaneous records of stresses in shank and fluke. The only existing results of some relevance are the presented results from the ramp test in the dry with 200 kg Dolosse.

It might be that these static test results can be representative with respect to influence of multi failure modes on the failure probability also for combined static and pulsating loads, but this must be verified. Until then it is proposed to use the static test result.

Correction for differences in surface roughness of the Dolosse

The flume tests reported in this paper were performed with the fairly smooth bronze filled polyester units, while prototype Dolosse are made of concrete, which gives a larger surface roughness. The difference has not been corrected for. Results from flume tests at AHL with 200 g model Dolosse made of mortar with the same surface roughness as prototype Dolosse are under way and will provide basis for a correction of the results presented in this paper.

Correction for bias due to fixed position of the instrumented section

It is unlikely that the instrumented section is the one where the largest principal tensile stress occurs in a given test at a given time. Although deviations might be small it must be noted that a one sided error (bias) is introduced, i.e. the recorded

results are on the unsafe side.

A quantification of this bias might be established from a comprehensive numerical simulation. Until then the effect is not taken into account and not corrected for in the presented results.

Correction for lack of shear and axial force components

The static test with 200 kg Dolosse on a ramp showed that in case of higher stress levels the negligence of shear and axial forces introduce a marginal error and is on the safe side. Consequently no correction is introduced in the flume test and the prototype test result is reported in the following.

Correction for the assumption of linear stress distribution

The calculations of the maximum principal tensile stress from component forces in the instrumented section are based on the assumption of linear stress distributions although it is known that the distributions generally are non-linear, sometimes with significant stress concentrations. The introduced error is believed to be two-sided but in most cases the results will be on the unsafe side. A quantification of this error has not yet been made, see discussion in Melby et al., 1990.

Results from the flume tests

Distribution of stress peaks for static plus pulsating loads

Preliminary design chart

Fig. 29 shows for three different sea states the stress distributions obtained from the flume tests with 200 g Dolosse only instrumented in one shank cross section. Results are from 6 positions of Dolosse within the area between levels SWL $\pm$ app. 1.5 times the Dolos height.

It is seen that the mean values (mean of ln) increase with the waveheight, but at the same time the standard deviation decreases. Consequently, the stress levels corresponding to higher exceedence probability levels are found to be almost invariant to the wave height for waves higher than a certain level.

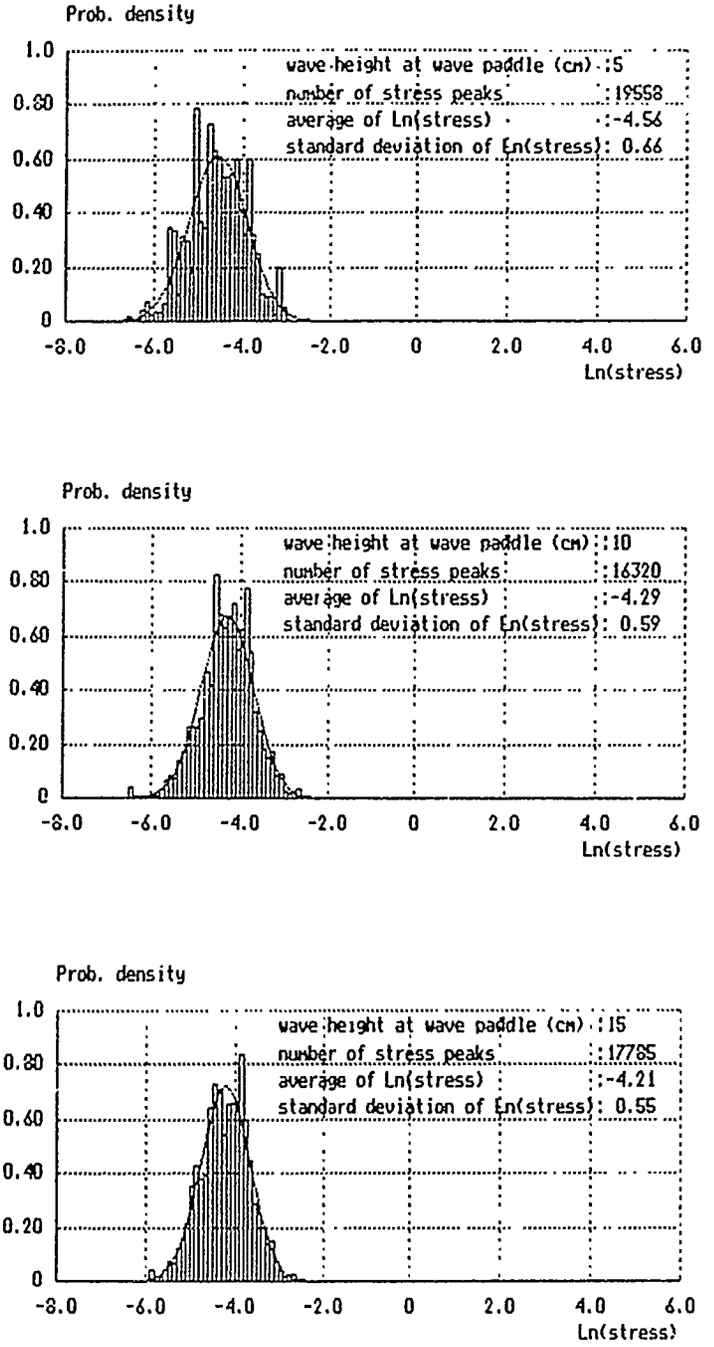

Fig. 29. Distribution of peaks static and pulsating stresses (in MPa).

Fig. 30 illustrates this tendency very clearly. The physical explanation of this might be that when exceeding a certain wave height the wave breaking will take place earlier on the armour slope which limits the wave heights of the acting waves, and consequently more waves will be of the same size. This tendency can also be seen in model test results with Tetrapods, Bürger et al., 1990.

Fig. 30 is an example of a preliminary design chart. Note that the static stresses (corresponding to zero wave height) are large compared with the total stresses under wave action.

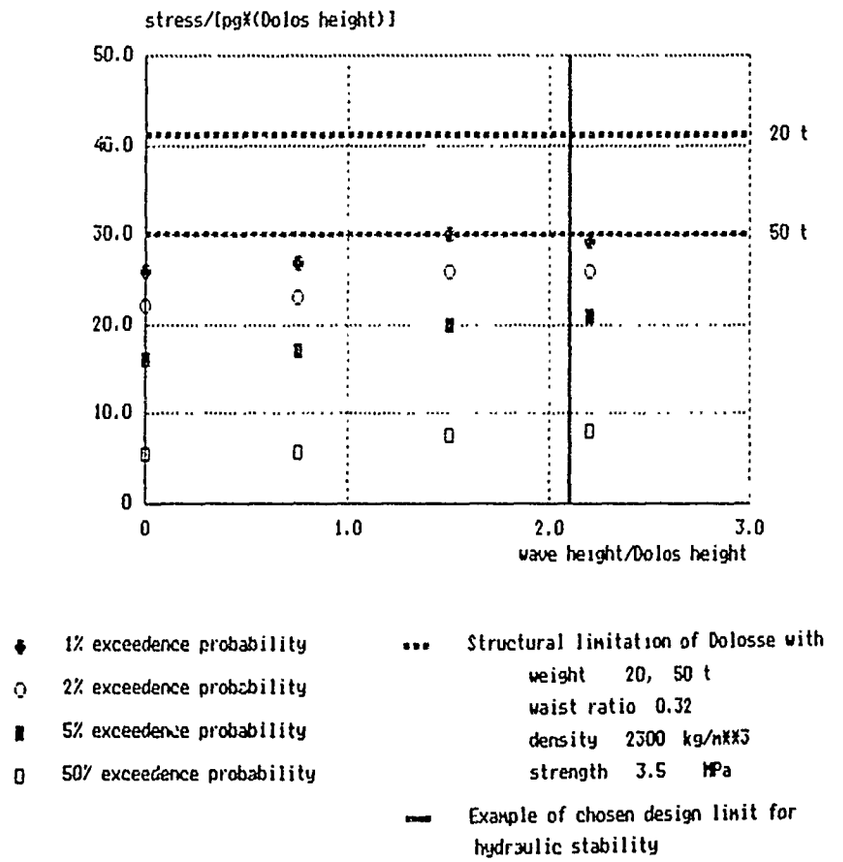

Fig. 30. Preliminary design chart for Dolos with waist ratio 0.32. The design chart covers the area between levels SWL ± app. 1.5 times the Dolos height. The exceedence probabilities are obtained from the fitted log-normal distribution of peaks of static and pulsating stresses. Impact stress, fatigue and the stress contribution from flukes are not included.

Static stresses recorded in flume tests

The distribution of the static stresses extracted from the flume tests is shown in Fig. 31. As is seen the distribution closely follows the log-normal distribution.

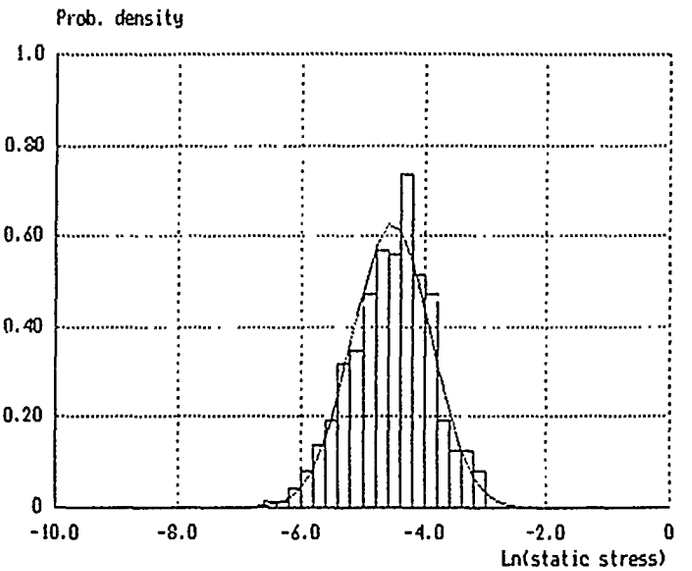

Static stress is defined as the average of the stresses of the 6 instrumented Dolosse before and after wave attack (MPa)

Wave height at wave paddle (cm)	:	5, 10, 15
Stress number	:	360
Average of Ln(static stress)	:	-4.54
Standard deviation of Ln(static stress)	:	0.64

Fig. 31. Distribution of static stresses in flume tests with 200 g Dolosse as recorded in one shank cross section.

Supplementary to Fig. 31 the relative importance of the averaged static stresses in the flume tests are shown in Fig. 32 as functions of the Dolosse position and the wave height.

	Pos. No of Dolosse / H^p_{m0} cm; $\bar{\sigma}_{static}/\bar{\sigma}$	5		10		15	
bottom layer	1	$\frac{0.015}{0.016}$	1.0	$\frac{0.016}{0.019}$	0.89	$\frac{0.017}{0.021}$	0.81
	2	$\frac{0.017}{0.019}$	0.89	$\frac{0.016}{0.021}$	0.76	$\frac{0.016}{0.023}$	0.70
	3	$\frac{0.014}{0.015}$	0.93	$\frac{0.017}{0.022}$	0.77	$\frac{0.018}{0.027}$	0.67
top layer	4	$\frac{0.009}{0.011}$	0.82	$\frac{0.009}{0.012}$	0.75	$\frac{0.01}{0.013}$	0.77
	5	$\frac{0.012}{0.016}$	0.75	$\frac{0.013}{0.018}$	0.72	$\frac{0.012}{0.018}$	0.67
	6	$\frac{0.006}{0.007}$	0.86	$\frac{0.007}{0.009}$	0.78	$\frac{0.008}{0.011}$	0.73

$\bar{\sigma}_{static}$ Average static stresses in 20 tests. The static stress is defined as the average of the static recorded before and after the wave action.

$\bar{\sigma}$ Average of peaks of total stresses in 20 tests.

The Dolosse positions are shown in Fig. 24.

Fig. 32. Relative importance of static stresses in flume tests with 200 g Dolosse as recorded in one shank cross section.

Distribution of pulsating stresses

The pulsating part of the various maximum principal tensile stress time series was extracted by removal of the time averaged values, i.e. $\bar{\sigma}_1$. As discussed before $\bar{\sigma}_1$ is generally different from σ_{static}, but the difference is small in case of dominant static stresses. Fig. 33 shows an example of the pulsating stresses.

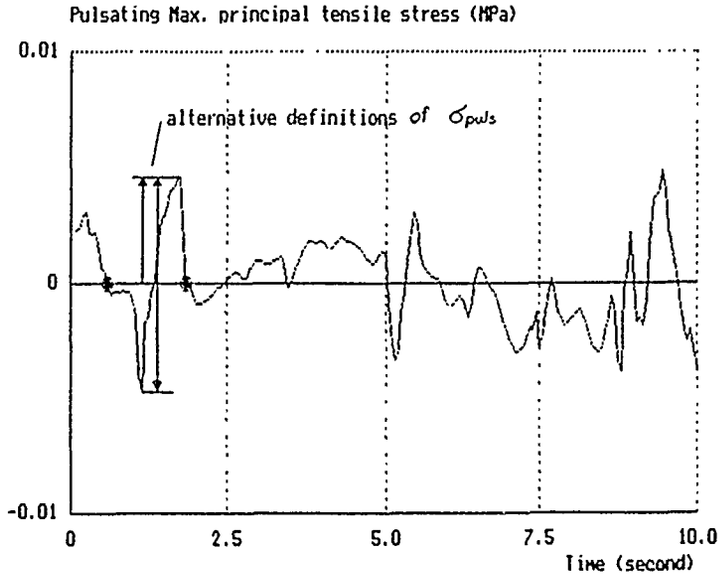

Fig. 33. Example of pulsating part of stress time series from flume tests with 200 g Dolosse at AHL.

For the statistical treatment $\sigma_{pulsating}$ is defined either as the maximum positive stress peak value within each "stress wave" identified by the zero down crossings or by the total height of the "stress waves". The two definitions are indicated in Fig. 33.

The first definition is relevant if the total stresses are to be calculated as the sum of the static and pulsating stresses.

The second definition using the total height of the stress waves are relevant for the estimation of fatigue effects. This definition is used in the analysis of the flume tests reported in the following.

The short term distribution of $\sigma_{pulsating}$ for the stationary 5 minutes time series was found to fit the Rayleigh distribution quite well, independent of the position of the Dolosse and the wave climate, Fig. 34. This indicates that a linear frequency

domain analysis where pulsating stresses are related to wave heights could be applied, Burcharth et al., 1988.

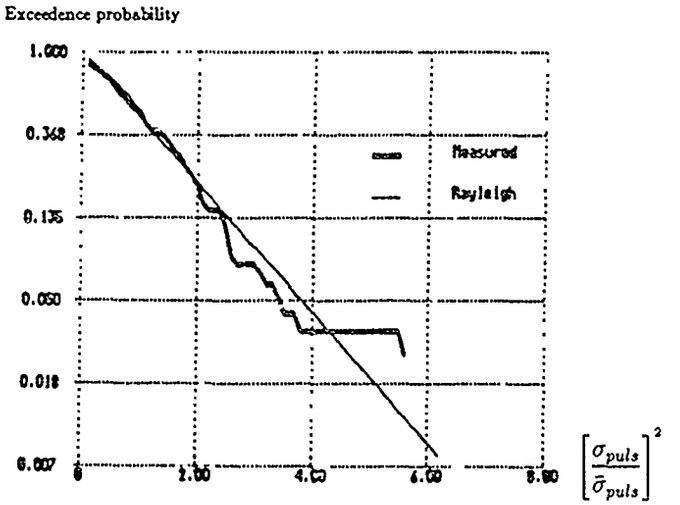

Fig. 34. Example of distribution of pulsating stress wave heights in a stationary sea state (short term distribution). Flume tests with 200 g Dolosse at AHL.

For the investigation of the dependency of pulsating stresses on wave climate and position of the Dolosse is used the characteristic value, $\bar{\sigma}_{puls\,1/10}$ defined as the mean of the highest one-tenth of the peaks, averaged over 20 repeated 5 minutes tests.

The results are shown in Fig. 35. Note that the wave heights are recorded at the toe of the breakwater.

Dolosse pos. / H^t_{m0} (cm) / $\bar{\sigma}_{puls\,1/10}$ (MPa)	bottom layer			top layer		
	1	2	3	4	5	6
5.7	0.006	0.0051	0.0061	0.0035	0.0038	0.0018
11.8	0.013	0.014	0.022	0.0071	0.008	0.0097
17.9	0.018	0.018	0.028	0.011	0.011	0.014

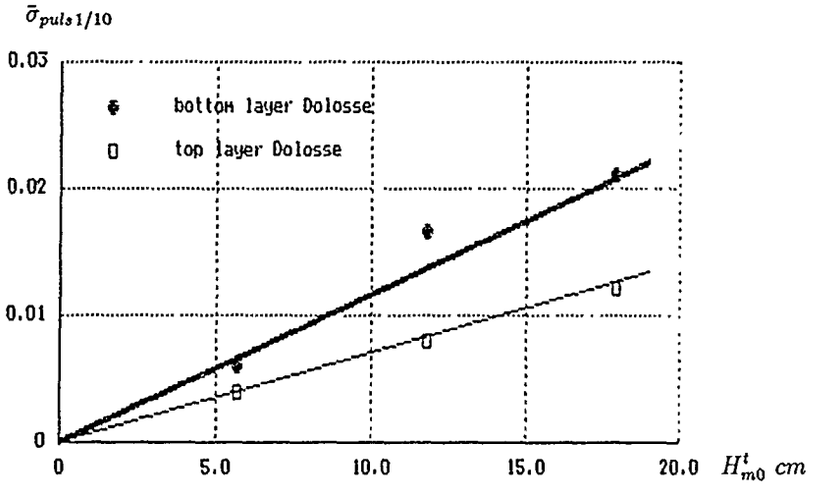

Fig. 35. Pulsating stress dependency on wave climate and Dolosse position. Flume tests with 200 g Dolosse at AHL.

As is seen the pulsating stresses increase with the wave height although the increase for higher sea states is rather weak, cf. also Fig. 31. The Dolosse in the bottom layer experience almost twice as high stresses as those in the top layer in terms of $\bar{\sigma}_{1/10}$. The physical explanation might be that more blocks can transfer wave generated force to a specific block situated in the underlayer compared with a specific block situated in the top layer.

The distribution of $\sigma_{puls\,1/10}$ follows the log-normal distribution quite closely . An example is shown in Fig. 36 which also gives the distribution parameters as functions of wave height and layer.

H_{m0}^t (cm)	bottom layer Dolosse		top layer Dolosse	
	μ	σ	μ	σ
5.7	0.76	0.83	0.35	0.52
11.8	1.91	0.68	1.41	0.40
17.9	2.25	0.56	1.79	0.40

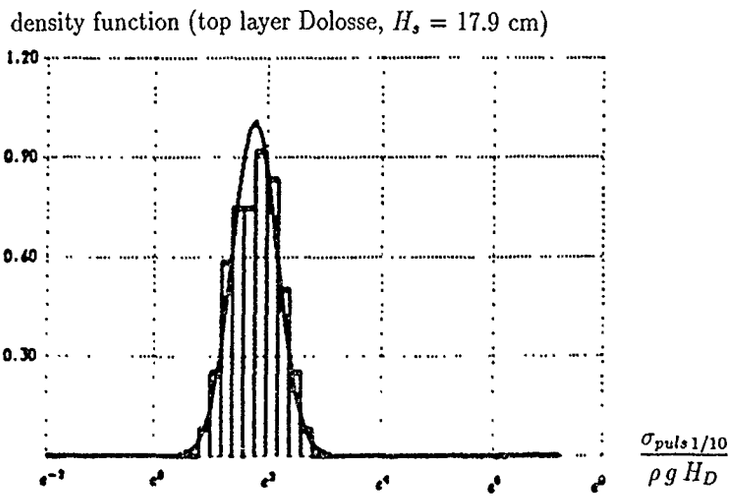

Fig. 36. Example of the distribution of $\frac{\sigma_{puls\,1/10}}{\rho g H_D}$ and the distribution parameters found in flume tests with 200 g Dolosse at AHL.

It is clearly seen that the distributions get significantly more narrow as the wave height increases. This effect is responsible for the similar but somewhat weaker tendency found for the sum of static and pulsating stress, cf. Fig. 29.

A linear relationship between a characteristic value of the pulsating maximum tensile stress, σ_{puls} and the wave height as illustrated in Fig. 35 was also found from the Crescent City Prototype study (Howell et al., 1990).

Fig. 37 shows the linear relationship between the mean of the maximum of σ_{puls}, $\bar{\sigma}_{puls\,max}$, for records of 30 minutes. $\sigma_{puls\,max}$ corresponds roughly to the 0.5% exceedence value. Note that in this study the definition of σ_{puls} corresponds to the first one mentioned in the explanation of Fig. 33.

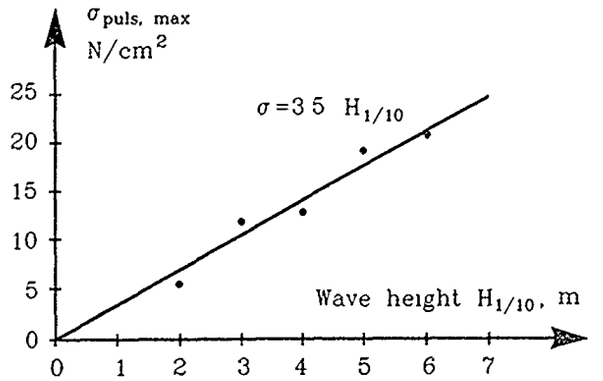

Fig. 37. Mean of maximum stress peak values in 30 minutes records of the pulsating stress in the 38 t Crescent City instrumented Dolosse (Howell et al., 1990).

Note that the factor 3.5 is dimensionless and invariant to the length scales because both H and σ_{puls} scale by length.

In the same study it was also found that $\sigma_{puls\,max}$ fitted reasonably well to the Rayleigh distribution using $\bar{\sigma}_{puls\,max}$ as the single parameter when the related sea states were classified into groups defined by ranges of $H_{1/10}$, $H_{1/10} = 1.5 - 2.5$ m, 2.5-3.5 m, ... 5.5-6.5 m.

Fig. 38 shows an example of the comparison of data with the Rayleigh distribution.

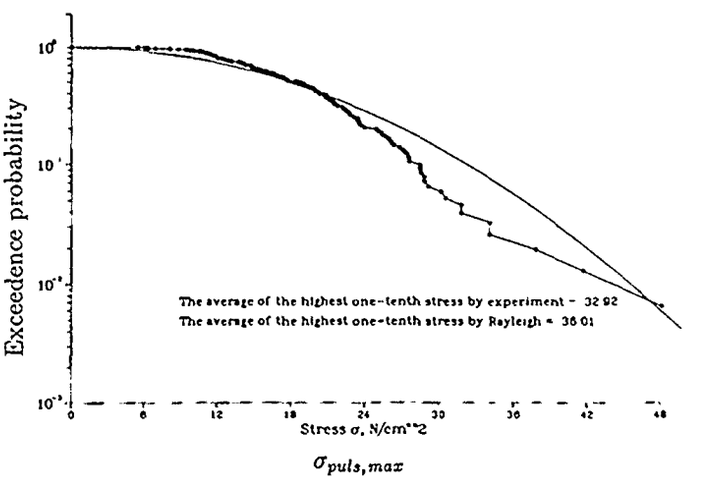

Fig. 38. Cumulative exceedence probability of the maximum values in 30 minutes records of the pulsating stress in the 38 t Crescent City instrumented Dolosse for $H_{1/10}$ = 4.5-5.5 m (Howell et al., 1990).

In general it was found that the Rayleigh distribution describes the lowest 90% of the data quite well and is conservative for the extreme values. The fit to the extreme values is rather poor for $H_{1/10} < 0.8\ H_D$ and is rather good for $H_{1/10} \geq H_D$, where H_D is the height of the Dolosse, i.e. the quality of the fit increases with the wave height.

It was demonstrated by CERC (Markle, 1990) in a 1 : 57.5 length scale model study of the Crescent City Breakwater that the response of the load cell instrumented 200 g Dolosse to wave loads compared very well to the recorded prototype data of the type shown in Figs. 37 and 38. This proves the feasibility of the research approach outlined in Fig. 3.

Fig. 39 shows the comparison between model and prototype data, and Fig. 40 illustrates the fit of the model data to the Rayleigh distribution.

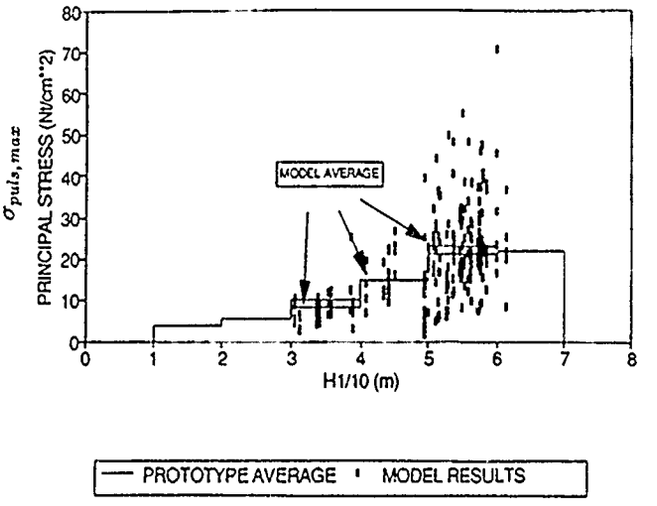

Fig. 39. Comparison of model and prototype results of recorded pulsating stresses. Crescent City Dolosse Study. (Markle, 1990).

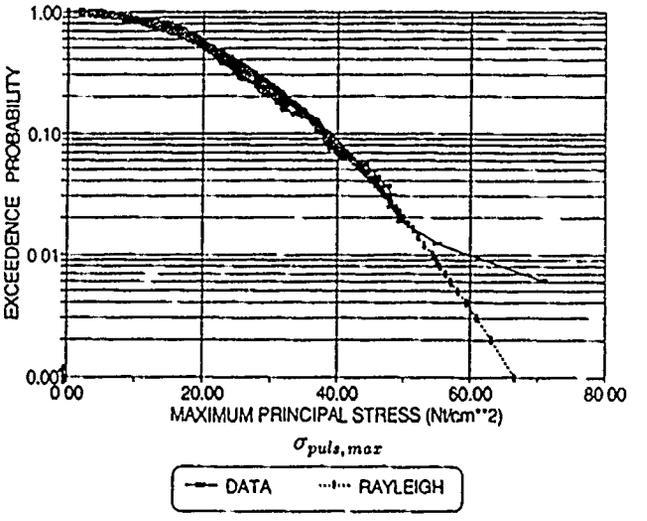

Fig. 40. Cumulative exceedence probability of maximum values of the pulsating stress recorded in a model study of the Crescent City Breakwater. Prototype values of $H_{1/10}$ = 5-6 m. (Markle. 1990).

Determination of impact stresses from small scale load cell instrumented Dolosse

From the formulae for Dolos impact stress, cf. Fig. 9, it can be derived that Dolos impact stress follows the scaling law

$$\lambda_\sigma = (\lambda_E \lambda_\rho \lambda_L)^{\frac{1}{2}} \tag{1}$$

where $\lambda_\sigma, \lambda_\rho, \lambda_L$ and λ_E are the scaling factors for impact stress, density, length and elastical modulus of the material. In principle eq (1) was derived through the use of the momentum equation

$$F\tau = m\,\Delta V$$

where	F	impact force
	m	mass of incident body
	ΔV	velocity difference of incident body before and after collision
	τ	impact time duration, taken to be proportional to the time elapse for a longitudinal wave to travel from the point of impact to a free edge of the structure and back again

As the speed of the stress wave is given by

$$C = \sqrt{\frac{E}{\rho}}$$

and the distance of travel is taken to be proportional to a characteristic length (e.g. the height of the Dolos H_D).

$$\tau \sim \frac{H_D}{C} = H_D\sqrt{\frac{\rho}{E}}$$

For two geometrically similar systems we then have the scale factor relationship

$$\lambda_\tau = \lambda_L \left(\frac{\lambda_\rho}{\lambda_E}\right)^{\frac{1}{2}}$$

According to the Froude Law (for constant gravitational acceleration)

$$\lambda_{\Delta V} = \lambda_L^{\frac{1}{2}}$$

Finally we obtain

$$\lambda_F = \lambda_L^{\frac{3}{2}} (\lambda_\rho \lambda_E)^{\frac{1}{2}}$$

and hence

$$\lambda_\sigma = \frac{\lambda_F}{\lambda_L^2} = (\lambda_E \lambda_\rho \lambda_L)^{\frac{1}{2}}$$

Consequently the scaling factor for impact-induced stress is related to Young's modulus of the material. Unfortunately, the inserting of a load-cell destroyes the homogenity of the material. This together with the ultra short duration of the stress pulse have prevented load-cell instrumented units from being used to study impact-induced stresses.

However, by comparing the results from large scale impact experiments (with Dolosse up to 30 t) with similar small scale impact experiments with the load-cell instrumented units and use of eq (1) it is possible to obtain an apparent Young's modulus for the latter ones. Such an apparent Young's modulus might then be used for the interpretation of impact signals recorded in small scale hydraulic tests.

The scale factor λ_E for Young's modulus in eq (1) is usually regarded independent of the size of the units and only a function of the material which is assumed to be elastic. However, in the case of large impacting units there might be some local crushing and spalling which tend to change the concrete from elastic to elastic-plastic response. In the large scale impact tests by Burcharth such local crushing and spalling took place especially in the drop test, but the results still confirm eq (1), in other words the effect seems to be negligible compared to the other sources of uncertainty. The reason for this minor importance is probably that in case of repeated impacts a locally crushed surface restitutes itself into an almost elastic behaviour.

With the aim of obtaining such an apparent Young's modulus of the instrumented 200 g polyester Dolos two kinds of impact tests were performed. The test set-ups exactly followed those suggested in Burcharth, 1981, cf. Fig. 9.

The impact signals of the Dolos were recorded by an analog - digital converter with 18,000 Hz base frequency (6,000 Hz for each channel). Fig. 41 is an example of the time series of the recorded signal in one of the bending moment channels.

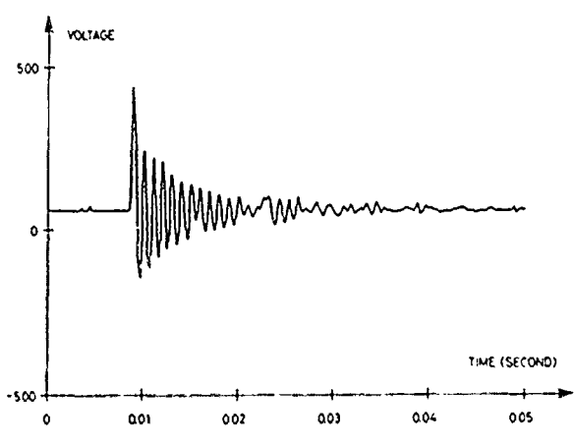

Fig. 41. Time series of impact signal.

To make the results comparable the results of the various prototype Dolosse with different waist ratios need to be transformed to the ones of the applied small scale 200 g Dolosse with the waist ratio of 0.32, because the Dolos waist ratio greatly affects its structural strength. This transformation can be done with the help of Burcharth's formulae, cf. Fig. 9. In the following is given the derivation of the transformation formula for drop test results.

Assuming there are two Dolosse, the prototype one with mass M_1 and waist ratio r_1 and the hypothetical one with mass M_2 and waist ratio r_2 . If the same angle of rotation applies for both Dolosse when rocking we get

$$\frac{\sigma_1}{\sigma_2} = \frac{1+r_1}{1+r_2}\left(\frac{r_2}{r_1}\right)^2 \left(\frac{E_1\rho g h_2}{E_2\rho g h_1}\right)^{\frac{1}{2}} \left(\frac{M_1 g h_1 H_{D_2}^3}{M_2 g h_2 H_{D_1}^3}\right) \tag{2}$$

If the Dolosse are made of identical concrete and experience the same stresses we obtain from eq (2) by applying Zwamborn's expression for the Dolos volume

$$V = 0.675\, r^{1.285} H_D^3 \tag{3}$$

$$\left(\frac{M_2}{M_1}\right)^{\frac{1}{6}} = \frac{1+r_1}{1+r_2}\left(\frac{r_2}{r_1}\right)^{0.93} \left(\frac{\sin(\alpha+\gamma_1)-\sin\gamma_1}{\sin(\alpha+\gamma_2)-\sin\gamma_2}\right)^{\frac{1}{2}} \tag{4}$$

The procedure of Dolos waist ratio transformation is summarized as followings:

(i) Given M_1 and r_1 of prototype Dolos and r_2 of hypothetical Dolos. If they are made of identical concrete and have the same stresses when dropped at the same rotation angle, the mass M_2 of the hypothetical Dolos is determined by eq (4).

(ii) calculate the height of the hypothetical Dolos by eq (3).

(iii) calculate the center lifted height of the hypothetical Dolos by eqs. of Fig. 9.

Table 3 lists the original and the transformed results of the prototype drop tests performed by Burcharth and Endo.

As no specific information on the dynamic Young's modulus and the tensile strength was given for Endo's tests average values for conventional concrete have been used in the analysis.

In Fig. 42a the dimensionless stress $\sigma_T/\sqrt{E\rho g H_D}$ is plotted against the dimensionless lifted height $\sqrt{h/H_D}$, where h is the lifted height of the center of gravity of the unit.

σ_T : Max principle tensile stress
E : Modulus of elasticity
ρ : Concrete density
H_D : Dolos height
h : Lifted height of gravitational centre of Dolos (in drop test) or pendulum (in pendulum test)
r : Dolos waist ratio

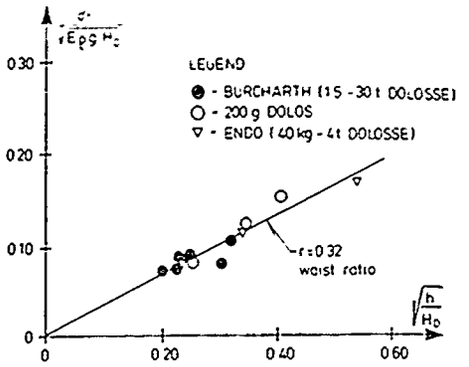

a) Drop tests

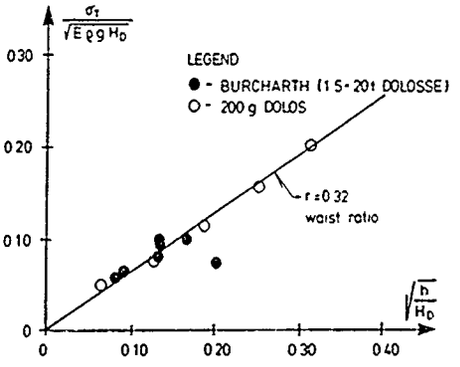

b) Pendulum tests

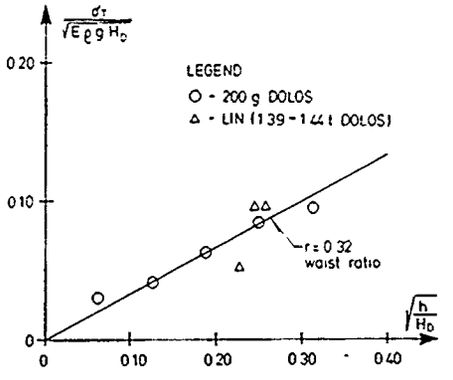

c) Transverse pendulum tests

Fig. 42. The result of impact calibration.

The apparent Young's modulus of the 200 g strain-gauged Dolos is

$$E = 9000 MPa \qquad \text{(drop test)} \tag{5}$$

Table 2 lists the original results of the prototype pendulum tests performed by Burcharth and the corresponding transformed results.

In Fig. 42b the dimensionless stress $\sigma_T/\sqrt{E\rho g H_D}$ is plotted against the dimensionless lifted height $\sqrt{h/H_D}$, where h is the lifted height of the pendulum.

The apparent Young's modulus of the 200 g strain-gauged Dolos is

$$E = 5000 MPa \qquad \text{(pendulum test)} \tag{6}$$

In both the drop and pendulum tests the Dolosse experience impacts mainly in one of the bending moment channels. A so-called transverse pendulum test, presented by Lin et al., 1986, cf. Fig. 43, was performed in order to study impact torsion response of the Dolos.

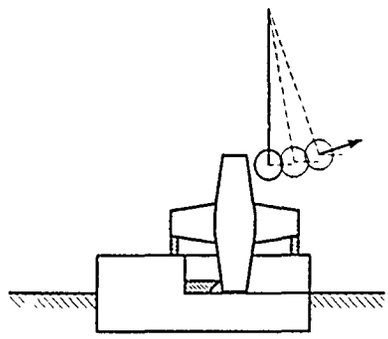

Fig. 43. The experiment set-up of transverse pendulum tests (For base dimensions see Fig. 9)

Table 5 lists the results of the prototype transverse pendulum tests performed by Lin.

In Fig. 42c the dimensionless stress $\sigma_T/\sqrt{E\rho g H_D}$ is plotted against the dimensionless lifted height $\sqrt{h/H_D}$.

The apparent Young's modulus of the 200 g strain-gauged Dolos is

$$E = 7000 MPa \qquad \text{(transverse pendulum test)} \qquad (7)$$

The three different apparent Young's moduli of 9,000 . 5,000 and 7,000 MPa for the impact loaded 200 g instrumented Dolos are fairly close on the background of the fact that the impact stress is proportional to the square root of the Young's modulus. Consequently, an average apparent value of $E = 7000\ MPa$ can be used with reasonable accuracy.

For other types of model armour units, a similar well defined test set-up and corresponding prototype results are a necessity in order to get apparent Young's modulus of model armour units to be used for impact calibration.

Table 3. Prototype and transformed results of drop test

	Burcharth (1981 a)						Endo (1984)		
	1	3	4	5	6	*	1	2	3
Dolos Mass M_1 (kg)	1500	1594	— 54000 —			30000	4000	400	40
Waist ratio r_1	— 0.303 —		— 0.35 —			0.37	— 0.32 —		
Dolos height (mm)	— 1650 —		— 2320 —			4050	2239	1038	482
Rotation angle	13.8°	15.7°	7.5°	7.3°	8.9°	5.7°			
Centre lifted height (mm)	153	171	117	115	138	297	120	120	140
Density ($kg/mm^3 \times 10^{-6}$)	2.33	2.47	— 2.4 —				2.28		
Dynamic Young's modulus ($N/mm^2 \times 10^4$)	3.6	7	5.2	4.96	4.5	4			
Tensile strength (N/mm^2)	2.95	5.74	4.38	3.56	4.18	4			
Dolos mass M_2 (kg)	1941	2067	3561	3561	3581	13551			
Waist ratio r_2	— — 0.32 — —								
Dolos height (mm)	1747	1750	2118	2118	2122	3307			
Centre lifted height (mm)	160	179	109	106	128.7	130			

Table 4. Prototype and transformed results of pendulum test

	Burcharth (1981 b)						
	1	3	4	5	6	7	8
Dolos Mass M_1 (kg)	1500	1594	— 54000 —			9740	19790
Waist ratio r_1	— 0.303 —		— 0.35 —			0.317	0.316
Dolos height (mm)	1650	1650	— 2320 —			3000	3800
Centre lifted height (mm)	46.5	45.8	40.5	39.9	39.9	23.2	23.2
Density ($kg/mm^3 \times 10^{-6}$)	2.33	2.47	— 2.4 —			2.31	2.31
Dynamic Young's modulus ($N/mm^2 \times 10^4$)	3.6	7	5.2	4.96	4.5	— 4.25 —	
Tensile strength (N/mm^2)	2.95	5.74	4.38	3.56	4.18	— 3.5 —	
Dolos mass M_2 (kg)	2822	2998	— 1914 —			10862	22891
Waist ratio r_2	— — 0.32 — —						
Dolos height (mm)	1979	1481	— 1722 —			3111	3989
Centre lifted height (mm)	79.5	55	30.1	29.6	29.6	21.1	24.4

Table 5. Prototype and transformed results of transverse pendulum test

	Lin (1986)		
	1	2	3
Dolos Mass M_1 (kg)	1390	1440	1440
Waist ratio r_1	0.319	0.329	0.329
Dolos height (mm)	1660	1660	1660
Centre lifted height (mm)	82	106	95
Density ($kg/mm^3 \times 10^{-6}$)	2.14	2.22	2.22
Dynamic Young's modulus ($N/mm^2 \times 10^4$)	3.6	4.3	4.3
Tensile strength (N/mm^2)	1.85	3.58	3.58
Dolos mass M_2 (kg)	1441	1045	1045
Dolos height (mm)	1627	1445	1445
Centre lifted height (mm)	83	96	86

Acknowledgement

The valuable asistance of Dr. L. Pilegaard-Hansen, Institute of Building Technology, University of Aalborg, in the early phase of the ramp tests is very much appreciated. Dennis G. Markle, Research Hydraulic Engineer, CERC, is acknowledged for his help during the first impact calibration of the small scale Dolosse.

References

Allsop, N.W.H., Hawkes, P.I., Jackson, F.A., Franco, L. : *Wave run-up on steep slopes - Model tests under random waves. Hydraulics Research.* Wallingford, Report No. SR2, August 1985.

Anglin, C.D., R.D. Scott, D.I. Turcke, M.A. Turcke : *The development of structural design criteria for breakwater armour units.* Proc. Seminar Stresses in Concrete Armor Units, ASCE, Vicksburg, U.S.A., 1990.

Burcharth, H.F. (1980) : *Full scale trials of dolosse to destruction.* Proceeding of the 17th International Conference on Coastal Engineering, 1980.

Burcharth, H.F. (1981a) : *A design method for impact loaded slender armour units.* Laboratoriet for Hydraulik og Havnebygning, Bulletin No.18, University of Aalborg, 1981.

Burcharth, H.F. (1981b) : *Full-scale dynamic testing of dolosse to destruction.* Coastal Engineering, Vol.4, 1981.

Burcharth, H.F. (1983) : *Comments on the paper by G.W.Timco titled "On the structural integrity of dolos units under dynamic loading conditions".* Coastal Engineering, Vol.7, No.1, Feb.1983.

Burcharth, H.F. (1984) : *Fatigue in breakwater armour units.* Proceeding of the 19th International Conference on Coastal Engineering, Houston, Texas, Sept. 1983.

Burcharth, H.F. (1987) : *The lessons from recent breakwater failures, development in breakwater design.* Invited Speech at World Federation of Engineering Organization Technical Congress, Vancouver, May, 1987

Burcharth, H.F. : *Full-scale dynamic testing of Dolosse to destruction.* Coastal Engineering 4, pp 229-251, 1981.

Burcharth, H.F., Brejnegaard-Nielsen, T. (1986) : *The influence of waist thickness of dolosse on the hydraulic stability of dolos armour.* Proceeding of the 20th International Conference on Coastal Engineering, Taipei, Taiwan, Nov. 1986.

Burcharth, H.F. and Gary Howell : *On methods of establishing design diagrams for structural integrity of slender complex types of breakwater armour units.* Seminaire International Entretien des Infrastructures Maritimes. Casablanca, Marocco, 1988.

Burcharth, H.F. and Liu Zhou : *A general discussion of problems related to the determination of concrete armour unit stresses including specific results related to static and dynamic stresses in Dolosse.* Proc. Seminar Stresses in Concrete Armor Units, ASCE, Vicksburg, U.S.A., 1990.

Bürger, H. Qumeraei, H.W. Partenscky : *Impact Strain Investigations on Tetrapods: Results of Dry and Hydraulic Tests.* Proc. Seminar Stresses in Concrete Armor Units, ASCE, Vicksburg, U.S.A., 1990.

DHL : Hydro Delft No 56, March 1980, Delft Hydraulic Laboratory, Holland, 1980.

Endo, T. (1985) : *Outline of study on structural strength of armour blocks.* Hydraulic Laboratory, Nippon Tetrapods Co., Ltd May, 1985

Hall, R.L. et al. : *Drop Tests of Dolos Armor Units.* Proc. of 1987 ASCE Structures Congress, Dynamics of Structures, August, 1987.

Howell, G.L. (1985) : *Crescent city prototype dolosse study.* Proceeding of Workshop on Measurement and Analysis of Structural Response in Concrete Armour Units, Vicksburg, Miss., USA, Jan. 1985

Howell, G.L. (1988) : *Measurement of forces on dolos armour units at prototype scale.* Proceeding of the 21st International Conference on Coastal Engineering, Spain, June. 1988

Howell, G.L. (1989) : *Stresses in Dolos armour units due to waves.* Seminar on structural response of armour units, Vicksburg, Miss., U.S.A., Nov. 1989

Howell, G., J.P. Rhee and J. Rosati : *Stresses in Dolos Armor Units due to Waves.* Proc. Seminar Stresses in Concrete Armor Units, ASCE, Vicksburg, U.S.A., 1990.

Hughes, S.A. : *The TMA shallow-water spectrum description and applications.* Technical Report CERC-84-7. Waterways Experiment Station, Vicksburg, Miss., U.S.A., 1984.

Ligteringen, H., H. Altink, J.H. van Orschot : *Strength of Concrete Armour Units: A Joint Industry Research.* Proc. Seminar Stresses in Concrete Armor Units, ASCE, Vicksburg, U.S.A., 1990.

Lillevang, O.J., W.E. Nickola : *Experiment studies on stresses within the breakwater armour pieces 'dolos'.* Proceeding of the 15th International Conference on Coastal Engineering, Honolulu, USA, 1976.

Lin, W.M., C. Rau, R.-L. Su : *The structural responses of dolos armour units under the dynamic loading.* Proceeding of the 20th International Conference on Coastal Engineering, Taipei, Taiwan, 1986.

Mansard, E.P.D., E.R. Funke : *The measurements of incident and reflected spectra using a Least Squares Method.* Proceeding of the 17th International Conference on Coastal Engineering, Sydney, Australia, March 1980.

Markle, D.G. : *Crescent City Instrumented Model Dolos Study.* Proc. Seminar Stresses in Concrete Armor Units, ASCE, Vicksburg, U.S.A., 1990

McDougal, W.G., J.A. Malby, J.W. Tedesco : *Wave forces on concrete armour units.* Journal of Waterway, Port, Coastal and Ocean Engineering, Vol. 114, No. 5, Sept. 1988.

Melby, J.A., G.L. Howell : *Incorporation of prototype Dolos static response in Dolos.* XXIII congress of international Association of Hydraulic Research, Ottawa, Canada, Aug. 1989.

Melby, J.A., B.T. Rossen, I.W. Tedesco : *An Analytical Investigation of Static Stresses in Dolosse.* Proc. Seminar Stresses in Concrete Armor Units, ASCE, Vicksburg, U.S.A., 1990

Nishigori, W., T. Endo, A. Shimeda : *On stress in tetrapods under wave action.* Proceeding of the 20th International Conference on Coastal Engineering, Taipei, Taiwan, Nov. 1986.

Sandstrom, A. : *Wave forces on blocks of rubble mound breakwaters.* Hydraulic Lab. Bulletins No. 83, Royal Institute of Technology, Stockholm, Sweden, 1974.

Scott, R.D., D.J. Turcke, W.F. Baird : *A unique instrumentation scheme for measuring loads in model dolos units.* Proceeding of the 20th International Conference on Coastal Engineering, Taipei, Taiwan, Nov. 1986.

Thoft-Christensen, P. and Y. Murotsu : *Application of Structural Systems Reliability Theory.* Springer Verlag, 1986.

Timco, G.W. : *The development, properties and production of strength-reduced model armour units.* Lab. Tech. Report, Nov. 1981. Hydraulics Lab. Ottawa, NRC, Canada.

Van der Meer, J.W., Pilarczyk, K.W. : *Dynamic stability of rock slopes and gravel beaches.* Proc. 20th Int. Conf. on Coastal Engineering Conference, Taipei, Taiwan, 1986.

Van der Meer, J.W. and G. Heydra : *Impact Velocities of Rocking Armour Units.* Proc. Seminar Stresses in Concrete Armor Units, ASCE, Vicksburg, U.S.A., 1990.

Zwamborn, J.A. and D. Phelp : *Structural Tests on Dolosse.* Proc. Seminar Stresses in Concrete Armor Units, ASCE, Vicksburg, U.S.A., 1990

Appendix A

Calculation of maximum principal tensile stress from cross sectional component forces obtained by load cell measurements

Failure is defined as occurring when the tensile stress at any point reaches the tensile strength of the unreinforced concrete.

It is observed from prototype Dolosse armour that fracture almost always occur as cuts through the shank or the flukes near the shank-fluke interfaces.

The stress conditions in these "critical sections" are 3-dimensional, but because the most critical stress conditions are known to occur at the surface of the body, it is a reasonable approximation to use a 2-dimensional stress failure criterion. The 2-D representation assumes that stresses caused by surface loads (contact forces between units) are negligible at the critical sections.

For the evaluation of the stress conditions in a cross section the 2-D principal stress failure criterion will be used:

$$f = -(\sigma_1 - S)(\sigma_2 - S) \leq 0 \qquad \text{(no failure)} \tag{A.1}$$

where σ_1 and σ_2 are the principal stresses, positive as tension, S is the tensile strength of the concrete.

Eq (A.1) is to be interpreted in such a way that σ_1 and σ_2 cannot simultaneously be larger than S without causing failure, cf. Fig. A.1.

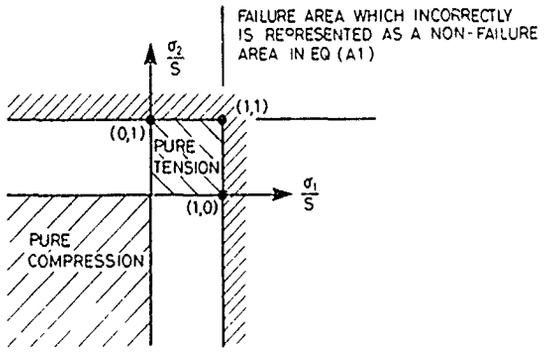

Fig. A.1. 2-dimensional principal stress failure criterion.

Failure will occur if either $\sigma_1 - S \leq 0$ or/and $\sigma_2 - S \leq 0$. It is then obvious

that failure occurs already when the largest of the two principal stresses exceeds S. Defining σ_1 as the largest, the adopted failure criterion is then

$$\sigma_1 \geq S \qquad \text{(failure)} \tag{A.2}$$

To evaluate the failure one has to find the maximum value of σ_1 for the specific cross section in question. According to the 2 D representation this maximum value of σ_1 occurs at the surface of the cross section for which reason only stress conditions at points on the surface are considered.

A local coordinate system as shown in Fig. A.2 is used

The x-coordinate is normal to section in question and the α-coordinate is parallel to the surface at the point of considerations. While the x-coordinate orientation is fixed relative to the cross section of the Dolos the α-coordinate shanges orientation dependent on the position of the point of analysis, P, given by the angle, θ.

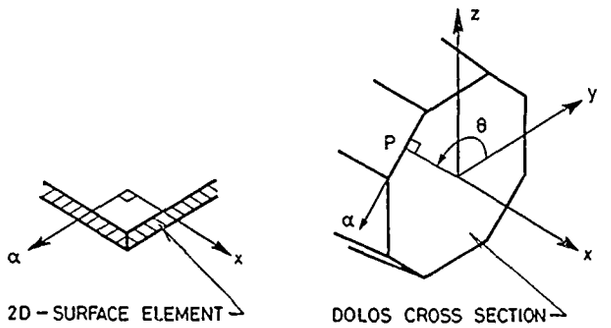

Fig. A.2. Coordinate system.

For simplicity a circular cross section is used as a close approximation to the octahedal cross section, Fig. A.3.

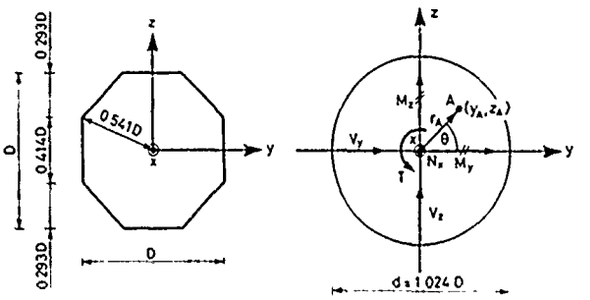

Areas of section

$$F = \pi \left(\frac{d}{2}\right)^2$$

Modulus of section

$$I_y = I_z = I = \frac{\pi}{64} d^4$$

Fig. A.3. Equivalent circular cross section.

The choise of the diameter, D of of the c ···lar section must be based on minimum deviation of the stresses at the surfaces. . ıding moments are supposed to be the dominant cross sectional force components. In case of pure bending, $d = 1.023\ D$, if the concrete is assumed linear elastic. Equivalent cross sectional areas are obtained for $d = 1.027\ D$ giving the same stress in case of pure axial forces. On this basis is chosen $d = 1.024\ D$.

It is assumed as an approximation that beam theory os applicable, i.e. the stress field in a cross section can be determinded from the cross sectional component forces shown in Fig. A.3.

M_z and M_y are the two components of the bending moment. V_z and V_y are the shear force components. T is the torque and N_x the axial force component.

The cross sectional force components are experimentally found from the recorded strains of the load cell.

The following notation is used for the orientation of the stress components: Take as an example σ_{xz}. The first subscript x indicates that the stress vector is acting in the plane perpendicular to the axis x. The second subscript z indicates that the stress vector is in the direction of the z axis.

For a circular section with diameter d, one can derive the following analytical expression for the stress components.

normal stress component in direction x

$$\sigma_{xx} = \frac{N_x}{F} + \frac{M_y}{I_y} z_A - \frac{M_z}{I_z} y_A \tag{A.3}$$

shear stress component in direction y

$$\sigma_{xy} = \frac{3+2\nu}{8(1+\nu)} \frac{V_y}{I_z} \left[\left(\frac{d}{2}\right)^2 - y_A^2 - \frac{1-2\nu}{3+2\nu} z_A^2 \right] - \frac{1+2\nu}{4(1+\nu)} \frac{V_z}{I_y} y_A z_A - \frac{T}{I_x} z_A \tag{A.4}$$

shear stress component in direction z

$$\sigma_{xz} = \frac{3+2\nu}{8(1+\nu)} \frac{V_z}{I_y} \left[\left(\frac{d}{2}\right)^2 - z_A^2 - \frac{1-2\nu}{3+2\nu} z_A^2 \right] - \frac{1+2\nu}{4(1+\nu)} \frac{V_y}{I_z} y_A z_A + \frac{T}{I_x} y_A \tag{A.5}$$

ν is Poisson's ratio

The formulae (A.4) and (A.5) fulfil the requirement that no stress component at right angle to the surface exists when only the above mentioned force components are present, i.e. no contact loads acting on the surface in the point of analysis.

At the surface eqs (A.3), (A.4), and (A.5) reduces to

$$\sigma_{xx} = \frac{N_x}{F} + \left(\frac{M_y}{I} sin\theta - \frac{M_z}{I} cos\theta\right) \frac{d}{2} \tag{A.6}$$

$$\sigma_{xy} = \frac{1+2\nu}{4(1+\nu)\,I} \left(\frac{d}{2}\right)^2 \left[V_y sin^2\theta - V_z sin\theta\, cos\theta\right] - \frac{T}{I_x} \frac{d}{2} sin\theta \tag{A.7}$$

$$\sigma_{xz} = \frac{1+2\nu}{4(1+\nu)\,I} \left(\frac{d}{2}\right)^2 \left[V_z cos^2\theta - V_y sin\theta\, cos\theta\right] + \frac{T}{I_x} \frac{d}{2} cos\theta \tag{A.8}$$

$I_x = 2I$ for the circular cross section.

With reference to the polar surface coordinate system given in Figs. A.2 and A.4 it is seen that the shear stress components σ_{xy} and σ_{xz} can be combined into

$$\begin{aligned} \sigma_{x\alpha} &= \sigma_{xz} cos\theta - \sigma_{xy} sin\theta \\ &= \frac{1+2\nu}{4(1+\nu)\,I} \left(\frac{d}{2}\right)^2 (V_z cos\theta - V_y sin\theta) + \frac{T}{I_x} \frac{d}{2} \end{aligned} \tag{A.9}$$

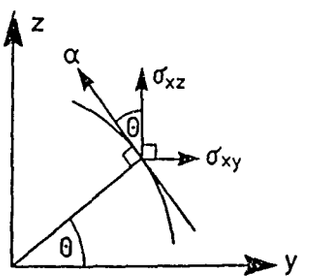

Fig. A.4.

Note that the stress component $\sigma_{\alpha\alpha}$ is zero if only the cross section force components given by N_x, M_y, M_z, V_y, V_z and T are present. Transforming these force components to equivalent stresses at the Dolos concrete surface gives of course no possibility of determining a stress component $\sigma_{\alpha\alpha}$. Such a component of some magnitude might exist if significant contact loads from neighbour Dolosse are present

at or near the section where the stresses are determined. However, because the most critical sections (i.e. sections where maximum tensile stresses are expected to occur) are known to be near the trunk-shank corners where contact points with other blocks are less likely to occur it is assumed that $\sigma_{\alpha\alpha}$ can be ignored.

The principal tensile stresses can be found from Mohr's diagram as follows, Fig. A.5.

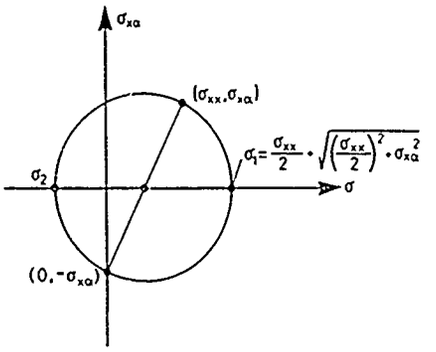

Fig. A.5. Mohr's diagram.

The largest of the two principal tensile stresses is found to be

$$\sigma_1 = \frac{\sigma_{xx}}{2} + \sqrt{\left(\frac{\sigma_{xx}}{2}\right)^2 + \sigma_{x\alpha}^2} \tag{A.10}$$

The angle, β between σ_1 and σ_{xx} in the surface plane is given in Fig. A.6.

$$tan2\beta = \frac{\sigma_{x\alpha}}{\frac{1}{2}\sigma_{xx}}$$

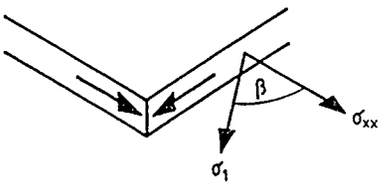

Fig. A.6. Illustration of orientation of σ_1.

Because failure occurs (cf. eq (A.2)) when the largest value of σ_1 exceeds S it is necessary to determine the maximum value of σ_1 at any given time.

σ_1 is a function of the polar coordinate θ (Figs. A.2 and A.3) at any given time, i.e. $\sigma_1 = f(\theta)$.

The *maximum principal tensile stress* is then determined from the equation

$$\left(\frac{\partial(f\theta)}{\partial\theta}\right)_{\sigma_1=max} = 0$$